

## The 3D Structure of the Virgo Cluster Region from Tully-Fisher and H I Data

José M. Solanes

*Departament d'Enginyeria Informàtica i Matemàtiques. Campus Sescelades, Universitat Rovira i Virgili.  
Alda. Països Catalans, 26; E-43007 Tarragona, Spain*

Teresa Sanchis and Eduard Salvador-Solé

*Departament d'Astronomia i Meteorologia and CER d'Astrofísica, Física de Partícules i Cosmologia,  
Universitat de Barcelona. Av. Diagonal 647; E-08028 Barcelona, Spain*

and

Riccardo Giovanelli and Martha P. Haynes

*Center for Radiophysics and Space Research and National Astronomy and Ionosphere Center<sup>1</sup>  
Cornell University; Ithaca, NY 14853*

jsolanes@etse.urv.es, (tsanchis,eduard)@am.ub.es, (riccardo,haynes)@astro.cornell.edu

### ABSTRACT

The distances and H I contents of 161 spiral galaxies in the region of Virgo cluster are used to gain insight into the complicated structure of this galaxy system. Special attention has been paid to the investigation of the suggestion presented in an earlier work that some peripheral Virgo groups may contain strongly gas-deficient spirals.

The three-dimensional galaxy distribution has been inferred from quality distance estimates obtained by averaging distance moduli based upon the Tully-Fisher relationship taken from eight published datasets previously homogenized, resulting in a relation with a dispersion of 0.41 mag. Previous findings that the spiral distribution is substantially more elongated along the line-of-sight than in the plane of the sky are confirmed by the current data. In addition, an important east-west disparity in this effect has been detected. The overall width-to-depth ratio of the Virgo cluster region is about 1 : 4, with the most distant objects concentrated in the western half. The filamentary structure of the spiral population and its orientation are also reflected by the H I-deficient objects alone. The H I deficiency pattern shows a central enhancement extending from  $\sim 16$  to 22 Mpc in line-of-sight distance; most of this enhancement arises from galaxies that belong to the Virgo cluster proper. However, significant gas deficiencies are also detected outside the main body of the cluster in a probable group of galaxies at line-of-sight distances  $\sim 25$ –30 Mpc, lying in the region dominated by the southern edge of the M49 subcluster and clouds W' and W, as well as in various foreground galaxies. In the Virgo region, the H I content of the galaxies then is not a straightforward indicator of cluster membership.

*Subject headings:* galaxies: clusters: Virgo — galaxies: evolution — galaxies: ISM — galaxies: spiral — methods: data analysis — radio lines: galaxies

---

<sup>1</sup>The National Astronomy and Ionosphere Center is operated by Cornell University under a cooperative agreement with the National Science Foundation.

## 1. Introduction

This article is the continuation of a series of papers on the HI content of spirals from the 21 cm line of neutral hydrogen data devoted to examine the extent to which the cluster environment influences the evolution of the galaxies.

The starting point, developed in Solanes, Giovanelli, & Haynes (1996, hereafter Paper I), was the establishment of reliable standards of HI mass for the various morphological subgroups of luminous spirals from a complete HI-flux-limited sample of these galaxy types in low density environments. That work was followed by a second paper examining the possible connections between gas deficiency and the properties of both the underlying galaxies and their environment in the fields of eighteen nearby clusters by Solanes et al. (2001, hereafter Paper II). The main motivation was to gain insight into the mechanisms responsible for the atomic gas depletion. While no clearly discriminating circumstances were found among those clusters which show significant HI deficiency and those which do not, this work definitely confirmed previous findings (e.g., Giovanelli & Haynes 1985; Haynes & Giovanelli 1986; Magri et al. 1988) that in HI-deficient clusters the proportion of gas-poor spirals increases monotonically towards the center. Moreover, Paper II clearly demonstrated, as first suggested by Dressler (1986), that HI-deficient objects move on orbits more radial than those of their gas-rich counterparts. This result made a strong case for the ram-pressure stripping of the spirals by the hot X-ray emitting intracluster medium (ICM) as the most likely process responsible for the gas deficiencies observed in rich cluster environments.

The wealth of 21-cm data gathered for the Virgo region in Paper II also made it possible to examine the distribution in two-dimensional space of the neutral gas deficiency in the Virgo central area. The sky distribution of HI deficiency was found to be in overall agreement with the radial pattern characteristic of rich clusters, showing that the maximum depletion occurred at the cluster center. But quite unexpectedly, the same map of the HI deficiency pattern, a variation of which is produced here as Fig. 1, also revealed peripheral groups of galaxies with a dearth of atomic hydrogen but found in areas where the density of X-ray luminous gas is very low, raising into question the feasibility that the ram-pressure of the ICM was responsible for the observed HI deficiency.

In the current paper, we conduct a further investigation into the nature of and conditions within the three-dimensional structure of the Virgo region, by incorporating into the analysis the HI content of its spiral population. The proximity of the region under study facilitates the gathering of a large number of 21-cm single-dish observations, which we complement with a large number of Tully-Fisher (1977, hereafter TF) distance estimates also reported in the literature. Section 2 presents a catalog of 161 galaxies with good HI and TF distance measurements. After reviewing in Section 3 the manner in which the HI deficiency is calculated, our galaxy sample is used in the following two sections to discuss, first the radial pattern of HI deficiency, and then its spatial distribution in the Virgo region. We conclude with a summary and some remarks in Section 7.

## 2. Observational Data

### 2.1. Galaxy Selection

The backbone of the present study is the complete spiral sample taken from the *Virgo Cluster Catalog* (Binggeli, Sandage, & Tammann 1985, hereafter VCC) by Yasuda, Fukugita, & Okamura (1997, YFO97) to study the Virgo cluster using the *B*-band TF relation. The YFO97 sample has been supplemented by

data from seven other studies of the Virgo cluster, likewise presenting TF distance estimates at various wavelengths. Table 1 lists the different sources of TF distances for Virgo objects included in the present work, along with the number of galaxies included in our catalog. These datasets include virtually all spiral galaxies used to date in the application of the TF relation to study the Virgo region.

For the current purpose, we have selected from the original catalogs listed in Table 1 only galaxies with heliocentric radial velocities below the well-defined gap near  $3000 \text{ km s}^{-1}$  that neatly isolates the Virgo region in redshift space (Binggeli, Popescu, & Tammann 1993). In addition, we have focused on galaxies located in the region bounded by  $12^{\text{h}} \leq \text{R.A.} \leq 13^{\text{h}}$  and  $0^{\circ} \leq \text{Decl.} \leq +25^{\circ}$  (throughout the paper equatorial coordinates are referred to the B1950.0 equinox), which encompasses the VCC survey boundary and is centered on the classical Virgo I cluster (de Vaucouleurs 1961). Thus, wherever we use the terminology “Virgo cluster region”, it should be kept in mind that objects located in the “Virgo Southern Extension” (Tully 1982) or Virgo II cluster, i.e., with  $\text{Decl.} < +5^{\circ}$ , are indeed largely excluded. Note that our selection procedure also implies that all the galaxies included in our sample (even those classified as background objects in VCC) are expected to have peculiar motions influenced by the central mass concentration of the cluster.

Our initial selection of Virgo galaxies includes a total of 198 objects, which we summarize in Table 2. This table contains, among other information, the distance moduli to each galaxy given in the eight TF studies on which our investigation is based. For seven of these galaxies, we also list their Cepheid distances given in the final results from the Hubble Space Telescope Key Project to measure the Hubble constant by Freedman et al. (2001) corrected for the effects of metallicity.

## 2.2. Homogenization of the distances to individual galaxies

Since our compilation of TF distances was built from eight datasets that contain sometimes inconsistent data, the average of the measurements available for each object does not necessarily provide the best estimate of the galaxy distances. We thus have attempted first to reduce the data to a homogeneous system by eliminating systematic differences among the different sources. We have carried out this task by means of a recursive procedure applied separately to each of the eight Virgo datasets listed in Table 1 and composed of the following steps:

(i) For each dataset, we take only those galaxies which also have distance measurements in any of the other seven datasets and calculate for each of those objects the arithmetic mean of all their distance estimates, as well as the standard deviation of the individual measurements.

(ii) Then, using only the galaxies in the chosen catalog which have multiple distance measurements, we determine the linear regression of the individual distances against the average values, applying a  $3\sigma$  clipping to remove those points which deviate significantly from the regression line. The regression coefficients are then recalculated and the  $3\sigma$  rejection procedure is repeated until no more galaxies are rejected. Once a datum is flagged as highly deviant, it retains this status for the rest of the procedure.

(iii) The regression coefficients calculated at the end of step (ii) are used to transform all distance measurements of the dataset under scrutiny, including those not listed elsewhere, into the system of mean distances defined by the sample members with multiple observations.

The standardization to the mean values affects each dataset differently. So once steps (i), (ii), and (iii) have been performed for the eight source catalogs (excluding the data already flagged as most deviant),

the procedure is repeated again until all the corrections become negligible. Convergence to a homogeneous system of mean distances is achieved in only a few cycles.

When *all* the distance measurements available for an individual object show residuals inconsistent with the regression lines, we ascribe this to a possible source misidentification and accordingly exclude the galaxy from the calculations. This seems to be the case of the galaxies V0975 and V1678, with only two distance measurements each that disagree beyond allowed uncertainty. We have also excluded from the homogenization process the seven galaxies with Cepheid distances: V0596, V1375, V1555, V1562, V1615, V1943, and N4725. For these galaxies we use the Cepheid measurements and their quoted errors.

The distances obtained with the procedure described above and their associated  $1\sigma$  uncertainties are listed in the last column of Table 2. The rms error of the individual distance moduli is 0.29 mag, which translates to an uncertainty of about 13% in the redshift-independent distance measurements. This means that for an individual galaxy at, say, 20 Mpc, we expect a typical error in the distance of  $\sim 2.5$  Mpc. This implies a sufficient level of accuracy in the measurement of individual distances to allow us to explore the gross features of the three-dimensional structure of the Virgo cluster.

### 2.3. The 21-cm sample

For the homogenization of the distance moduli, we have taken all the galaxies listed in two or more of the source TF catalogs (i.e., with multiple distance measures), regardless of their Hubble type, in order to minimize the impact of statistical “shot noise”. Since irregular and bulge-dominated galaxies may give, however, unreliable TF distances and/or HI content measurements, we re-examined the morphologies of the galaxies and picked up only those with Hubble types ranging from  $T = 1$  (Sa) to  $T = 9$  (Sm), as given in the *Third Reference Catalogue of Bright Galaxies* (de Vaucouleurs et al. 1991, hereafter RC3).

The principal source for the HI line fluxes is the *Arecibo General Catalog* (hereafter AGC), a private database maintained by RG and MPH, which contains an extensive compilation of 21-cm-line measurements collected from a large number of sources. Among the galaxies with a clear spiral morphology, there are 15 for which the AGC did not provide useful data, including 2 galaxies that overlap with obvious optical companions and 3 non-detections. We found HI flux measures for 9 of these objects in *A General Catalog of HI Observations of Galaxies* (Huchtmeier & Richter 1989) and in the *Lyon-Meudon Extragalactic Database* (LEDA). All the observational values have been corrected for the effects of random pointing errors, source extent, and internal HI absorption following Haynes & Giovanelli (1984), except the nine non-AGC fluxes and the only non-detection, V0522, which have been corrected only for internal HI self-absorption and assigned an ‘H’ flag in the final dataset.

The AGC is also adopted as the source of other observational parameters required by our study, such as the equatorial coordinates of the galaxies, their visual optical diameters, which are involved in the determination of the HI deficiency (see next section), and their heliocentric radial velocities, which we transform to systemic velocities,  $v_{\text{sys}}$ , by referring them to the kinematic frame of the Local Group, taken equal to  $308 \text{ km s}^{-1}$  towards  $(l, b) = (105^\circ, -7^\circ)$  (Yahil, Tammann, & Sandage 1977).

On the other hand, for the HI-line width, a parameter of lesser importance in this investigation, the heterogeneity of the measures contained in the AGC prompted us to adopt instead the inclination-corrected values of the line width at 20% level of the line-profile peak,  $W_{20}^c$ , listed in YFO97. For most of the galaxies that concern us here, these authors provide a set of observations standardized into line widths measured

at the Arecibo circular feed following a similar process to that carried out here with the distance moduli. For galaxies not included in the YFO97 sample, we use the values of  $W_{20}$  and inclination quoted in LEDA, except for the galaxy V1043, not listed in either of these two catalogs, for which we adopt the corresponding measurements by MAH80 (measurements other than from YFO97 are flagged 'W' in the final dataset). Furthermore, we have excluded spiral galaxies with  $W_{20}^c \leq 100 \text{ km s}^{-1}$  to reduce the error induced from turbulent disk motion. We do not impose an inclination cut because this parameter does not play any explicit role in our investigation (remember that, for most of the galaxies in our dataset, we are adopting values of the line width already corrected for inclination). Nevertheless, objects with  $i < 45^\circ$  in LEDA are warned with an 'i' flag in our final catalog.

After all these selections, we end up with a sample of 161 spiral galaxies with reliable HI content and distance data, hereafter called the “21-cm sample”, which is used below to assess the spatial distribution of the neutral gas deficiency in the Virgo cluster region. As stated in § 4, the scatter of the best fitting TF template for the 161 galaxies is 0.41 mag. Hence, the uncertainty in the distance modulus of the individual galaxies in this dataset is comparable to the scatter of the most accurate TF template relations currently available.

All the parameters relevant to our investigation are listed in Table 3, where we have included two different measurements of the HI deficiency and the absolute  $B$ -magnitude of the galaxies,  $M_{B_T}^c$ , calculated from their total apparent corrected  $B$ -magnitude listed in LEDA and our distance estimate. The sky distribution of the members of the 21-cm sample is presented in Figure 1.

### 3. The Diagnosis of HI Deficiency

HI deficiency is often quantified by the parameter  $\langle DEF \rangle$  defined as

$$\langle DEF \rangle = \langle \log M_{\text{HI}}(D_{\text{opt}}, T) \rangle - \log M_{\text{HI}} , \quad (1)$$

(e.g., Chamaraux, Balkowski, & Gérard 1980; Haynes & Giovanelli 1984; Paper I), where  $M_{\text{HI}}$  is the HI mass of the galaxy in solar units, and the angular brackets on the right of the equal sign indicate the expected value of this quantity inferred from a sample of field galaxies of the same *optical* linear diameter  $D_{\text{opt}}$  and morphological type  $T$ . The most recent determinations of the expectation values for the HI mass as a function of the size and morphology of the galaxies are given in Paper I in the form of linear regressions that imply power law relationships of the type  $M_{\text{HI}} \propto D_{\text{opt}}^n$ , with the values of  $n$  oscillating between about 1.7 for Sc's and 1.2 for earlier spiral types.

For the present study, however, we need to use a calibrator for the neutral gas deficiency not tied to the distance to the galaxies. Given that the  $M_{\text{HI}} - D_{\text{opt}}$  relationships do not deviate substantially from a constant HI surface density, especially for the latest spiral types, it is reasonable to adopt the distance-independent approximation to equation (1) based on the difference of the logarithms of the expected and observed values of this latter quantity

$$DEF = \langle \log \bar{\Sigma}_{\text{HI}}(T) \rangle - \log \bar{\Sigma}_{\text{HI}} , \quad (2)$$

where  $\bar{\Sigma}_{\text{HI}}$  is the mean *hybrid* HI surface density, which can be calculated directly from the ratio of the observables  $F_{\text{HI}}$  and the apparent optical diameter of the galaxy,  $a_{\text{opt}}^2$ , given in arcmin (see also Paper I). The adopted values for  $\langle \log \bar{\Sigma}_{\text{HI}}(T) \rangle$  are: 0.24 units for Sa, Sab; 0.38 for Sb; 0.40 for Sbc; 0.34 for Sc; and 0.42 for later spiral types.

The values of HI deficiency for the galaxies of the 21-cm sample calculated using the two definitions given above are listed in columns (4) and (5) of Table 3 —to gauge the numerical values, they can be compared with the overall scatter of 0.24 units shown by field galaxies (Paper I). A brief glance at the figures shows that the two measurements are indeed very close for most galaxies. Hence, statistical measurements of the HI deficiency that rely on values of DEF taken from subsets of objects not segregated according to size should give unbiased estimates of this property. We note also that the error in  $\langle DEF \rangle$  resulting from the propagation of the uncertainty in the distance modulus (see § 2.2) is equal to 0.079 units for an Sb galaxy, while the model scatter is equal to 0.126 units. This means that a substantial portion of the error budget of this model can be attributed exclusively to the uncertainty of the galactic distances.

#### 4. Possible Bias of HI Deficiency in the Distance

A potential problem with the determination of TF distances from HI line widths, first brought into consideration by Guhathakurta et al. (1988) and Teerikorpi et al. (1992), results from the possibility that gas stripping can reduce the size of the HI disks to radii smaller than the turnover of the rotation curve (see, e.g., Cayatte et al. 1994). This would produce objects that are too luminous for their line width, therefore resulting in TF distances that are artificially underestimated. Possible evidence of this effect has been cited in the Virgo cluster studies by Fukugita et al. (1993), YFO97, and FTS98, though no environmental dependences on TF distance determinations have been found in more distant clusters (Giovanelli et al. 1997; Dale et al. 2001) using combined HI and optical rotation width datasets.

We have investigated the possible alteration of distance resulting from atomic gas deficiency in our Virgo data by inspecting the positions of the members of the 21-cm sample on the  $M_{B_T}^c$ - $\log W_{20}^c$  plane (i.e., the TF relation) according to their HI deficiency. The two linear regressions of the data excluding HI-deficient objects (i.e., those with  $DEF \geq 2\sigma$ ) are:  $M_{B_T}^c = -6.75 \log W_{20}^c - 2.55$  and  $\log W_{20}^c = -0.13 M_{B_T}^c - 0.05$ . More importantly, the number of gas-poor galaxies on each side of the regression lines is about the same. Similar behaviors are obtained when the threshold for the exclusion of the HI-deficient objects is increased up to 3 and 4 $\sigma$  (the latter value implying roughly a factor 10 decrement in the HI mass), with regression lines obeying equations almost identical to the former ones. These results are consistent with a scenario in which the gas deficiency does not have any noticeable effect on the distance estimates, even for the objects most severely depleted in their interstellar HI gas. This conclusion is also supported by the observation that for the data points corresponding to the most HI-deficient galaxies the values of  $\langle DEF \rangle$  do not appear to be systematically lower than those calculated from the distance-independent parameter DEF.

The absence of systematic deviations from the mean values of the TF relation with increasing gas deficiency suggests that, in any event, the value of the distance underestimates that could affect our most HI-deficient galaxies should be commonly smaller than the rms residual about the regression line, which has a value of 0.41 mag (i.e., should be lower than 19%). We note that this scatter is only slightly larger than the values around 0.35 mag found in TF templates based on the combination of measurements in many clusters (e.g., Gav99, Dale et al. 1999) and fully comparable to the intrinsic scatter of 0.43 mag found by Sakai et al. (2000) for nearby galaxies with Cepheid distances.

## 5. The HI Deficiency in Virgo

Numerous studies (e.g., Giovanelli & Haynes 1985; Haynes & Giovanelli 1986; Magri et al. 1988; Cayatte et al. 1994; Bravo-Alfaro et al. 2000) reveal that gas-poor galaxies tend to be more abundant in the centers of rich galaxy clusters than in their periphery. Virgo is less rich and younger than the classical Abell clusters and is characterized by a lower X-ray luminosity and larger spiral fraction than Coma-like clusters. Probably as a result, although it does contain a substantial fraction of HI-deficient galaxies (e.g., Haynes & Giovanelli 1986; Paper II; see also below), the degree of HI deficiency is not observed to increase towards the center as dramatically as in other rich clusters. However, because of its proximity, even strongly gas-poor galaxies remain detected, allowing precise determination of higher degrees of the HI-deficiency, whereas in more distant clusters only lower limits to this parameter can be derived.

The contour map of HI deficiency shown in Figure 1 illustrates that the maximum of the gas deficiency distribution coincides with the position of the central cD galaxy, M87, where the projected galaxy and intracluster gas densities are also the highest. But this map also reveals other zones of significant deficiency at sky positions dominated by background subclumps which lie at substantial clustercentric distances.

### 5.1. Radial Pattern

The first lines of evidence that there is an excess of highly deficient galaxies on the outskirts of the Virgo cluster are presented here by means of Figures 2 and 3. Figure 2 shows the values of DEF for the 161 members of the 21-cm sample as a function of their line-of-sight (LOS) distance,  $d$ . This diagram illustrates that most of the galaxies with substantial deficiencies in the Virgo cluster region are localized in a broad range of projected distances, which stretches from about 10 to 30 Mpc along the LOS. A few more gas deficient objects lie beyond 40 Mpc.

By transforming the sky positions of the galaxies and their LOS distances to rectangular coordinates, we can also inspect the behavior of the HI deficiency as a function of the *three-dimensional* radial distance,  $r$ , from the center of Virgo. We adopt the standard identification of the cluster center at the position of M87, given by the sky coordinates ( $12^{\text{h}}28^{\text{m}}3$ ,  $12^{\circ}40'$ ) and a distance modulus of 31.11 mag quoted in LEDA, which translates to a LOS distance of 16.7 Mpc. The results are shown in Figure 3, where we adopt two different representations of the radial run of the HI deficiency: one based on the parameter  $F_{\text{DEF}}$  used in Paper II, which measures the relative populations of deficient and normal spirals, and the other based directly on the averaged values of DEF. In both cases the data have been binned into annuli containing 16 galaxies per ring, with the final bin having 17, in order to increase the statistical weight of the scarcer low- and high-distance objects.

We see that, for  $r \lesssim 4$  Mpc, the radial behavior of the gas deficiency is consistent with the pattern exhibited by the composite sample of 11 HI-deficient clusters investigated previously in Paper II (see Figure 4 therein): it decreases almost monotonically towards normalcy with increasing distance from the cluster center. But at greater Virgocentric distances this tendency is broken by a series of secondary maxima, more conspicuous in the radial run of  $F_{\text{DEF}}$  because of its higher sensitivity to localized enhancements, caused by regional enhancements of gas deficiency where this parameter reaches values several times larger than —and clearly inconsistent with— the field expectation ( $\sim 2\text{--}3\%$ ). Besides, as illustrated in Figure 2, the spirals on the Virgo cluster outskirts are not only more likely to be deficient in HI than field objects, but they also reach gas deficiencies typical of the cluster core. The reader, however, should be aware of the fact that this same sort of careful analysis of HI deficiency at large clustercentric distances has not been performed on

other clusters. So, it is not unfeasible that the differences in the radial pattern can be explained simply by the bias that arises from Virgo’s proximity which leads to (a) much larger number of 21-cm observations, (b) more stringent values of DEF, and (c) more accurate TF distance estimates.

Further inspection of Figure 2 (see also § 6.1) reveals that the central peak in the radial pattern of the HI deficiency is the result of the accumulation of highly deficient galaxies in the interval of LOS distances ranging from  $\sim 16$  up to 22 Mpc. This range coincides essentially with the distribution of the bright ellipticals associated with the cluster core (Neilsen & Tsvetanov 2000). The second local maxima visible in the radial run of  $F_{\text{DEF}}$  is produced by galaxies with extreme deficiencies at  $d \lesssim 15$  Mpc, while the peak most distant from the cluster core obeys to several gas-deficient objects at LOS distances between about 25 and 30 Mpc. As we show in the next section, this latter enhancement of HI deficiency might be related to one of the classical background clouds of the Virgo cluster region.

Previous studies by Fukugita, Okamura, & Yasuda (1993), YFO97, and FTS98, among others, have shown that the Virgo spiral distribution is strongly elongated along the LOS. The impressions obtained above from the distribution of HI deficiency, although crude, provide further evidence for the large depth in LOS distance of the Virgo spirals, which we now see that is also reflected in the gaseous deficiency. Hence, in contrast to what it is commonly assumed, not all the HI-poor objects in the Virgo region reside in the neighborhood of the cluster core.

## 5.2. Correlation with Recessional Velocities

The most frequently discussed gas removal mechanism that depends on the ICM density is ram-pressure sweeping (Gunn & Gott 1972; Quilis et al. 2000; Vollmer et al. 2001). For a given galaxy, the stripping efficiency relies both on the density of the hot intracluster gas and on the square of the relative velocity of the galaxy with respect to the latter (actually, it is only the component in the direction normal to the disk that matters). Suggestive indication that it is a density that correlates with gas deficiency is provided by the radial nature of the deficiency pattern in the core of rich clusters (see Paper II), which, as shown above, it is also reproduced in the center of the Virgo cluster region. However, attempts to unearth further evidence of ram-pressure stripping by seeking possible correlations between HI depletion and velocity relative to the cluster are severely limited, not only by projection effects arising from the poor correlation between the unknown space velocities of the galaxies with the one component that can be measured (see, e.g., Giovanelli & Haynes 1985; Haynes & Giovanelli 1986; Magri et al. 1988), but also because in some cases the effects of the galaxy-ICM interaction are observed only *after* the closest passage of the galaxies to the cluster center (Vollmer et al. 2001).

The inclusion of 2D or 3D positional information increases notably the sensitivity of the tests. In Paper II, this approach served to demonstrate that spirals devoid of gas follow more eccentric orbits than the gas-rich objects in the central regions of HI-deficient clusters. However, in the dynamically young Virgo cluster, where the galaxy orbits are not yet fully settled, no correlation was found between the gas deficiency and the orbital parameters of the spirals. A similar exercise is reproduced here in Figure 4 for a much more spatially extended dataset. This figure shows the radial velocities of the galaxies in our 21-cm sample relative to the Virgo systemic velocity—for this parameter we choose the typical value of  $980 \text{ km s}^{-1}$  (e.g., Teerikorpi et al. 1992)—plotted as a function of their right ascension and LOS distance for different intervals of HI deficiency. As in the previous study of the central Virgo region, the inspection of the different panels does not reveal any clear connection between the kinematics of the galaxies and their gas contents. An indication



exists that the galaxies with  $\text{DEF} = 2\text{--}3\sigma$  closest to the cluster core have preferentially higher relative velocities. This impression, however, is not corroborated by the objects with the highest gas deficiencies. The only clear trait, consistently repeated in the four panels, is the coherence in sign and in magnitude of the relative velocities of the galaxies located at large Virgocentric distances, suggesting collective motions that still retain a memory of the Hubble expansion: galaxies behind the Virgo core ( $d \gtrsim 30$  Mpc) tend to move far away at high speed, while almost all galaxies in front of this region ( $d \lesssim 15$  Mpc) exhibit substantial radial movements toward us. The feasibility of a scenario in which the galaxies at large Virgocentric distances are deficient from having traversed the cluster core earlier is explored in Sanchis et al. (2002).

The inclusion of spatial coordinates perpendicular to the LOS in the present graphical analysis serves to emphasize additionally the marked east-west asymmetry in the depth of the galaxy distribution. In the western half of the Virgo cluster region, most galaxies have LOS distances spread throughout the range from 10 to 50 Mpc, whereas, in the eastern half, few objects are seen at distances larger than 25 Mpc. Interestingly enough, West & Blakeslee (2000) also detected a tendency for the brightest elliptical galaxies located in the western region of the Virgo cluster to be more distant than those on the eastern side. In contrast, as evident in Figure 1, the X-ray emission of the cluster core is more extended towards the eastern side.

## 6. The Three-Dimensional Structure of the Virgo Region

Some progress toward a precise determination of the complex structure of the Virgo cluster region is now beginning to emerge from distance measurement methods capable of determining individual galaxy distances to a precision comparable to the inter-group separations. Recent studies relying on TF, surface brightness fluctuations, or fundamental plane distance measurement techniques (e.g., YFO97; Gav99; Neilsen & Tsvetanov 2000; Fouqué et al. 2001) have produced quite an elaborate set of substructures and opened a debate on the original group membership assignments of numerous galaxies. In essence, however, they have confirmed the robustness of the original subdivision inferred from imaging and recessional velocity data (e.g., de Vaucouleurs 1961; VCC; Binggeli et al. 1993) that splits the Virgo I cluster region essentially in two major central subclusters and three peripheral groups (cf. Fig. 1). The largest galaxy concentration dominates the northern part of the Virgo region and coincides with the brightest giant elliptical, M87, which also appears to be the center of the X-ray emission (Böhringer et al. 1994). This main subunit, which will be referred to here as the M87 subcluster, is supposed to trace the cluster core, which might not be virialized (Binggeli et al. 1993; Böhringer et al. 1994; Schindler, Binggeli, & Böhringer 1999). Another giant elliptical, M49, marks the center of the other major Virgo galaxy concentration, hereafter the M49 subcluster, located southwards from the M87 subcluster. The M49 subcluster appears to be connected towards the southwest with the  $W'$  and  $W$  background clouds (de Vaucouleurs 1961), forming a continuous chain that extends up to roughly twice the distance of the M87 subcluster (interestingly enough, a tenuous bridge of X-ray luminous gas can be seen in Fig. 1 connecting the M49 subcluster with the  $W'/W$  cloud region). Finally, in the northwest and at about the distance of the  $W$  cloud, there is another well-defined background cloud named  $M$  (Ftclas, Struble, & Fanelli 1984).

### 6.1. Spherical Coordinates

Let us see now whether the main substructures of the Virgo region that we have just enumerated bear any relationship with any of the maxima observed in the radial pattern of the HI deficiency. For this, we use

the tomographic presentation of the sky distribution of the members of the 21-cm sample shown in Figure 5 which partitions the galaxies into 9 segments of TF distance.

It is seen clearly that the center of gravity of the HI deficiency distribution moves from north to south as the distance increases, consistently following the structure of the Virgo cluster described above. The major concentration of HI-deficient spirals is seen in the distance range of 15–20 Mpc encircling the position of M87. Numerous gas-deficient objects are detected also in the panels corresponding to the distance ranges of 10–15 Mpc and 25–30 Mpc. In the latter, these galaxies are essentially concentrated between the southern edge of the M49 subcluster and the W'/W cloud region, while in the former they tend to be located to the north of M87. Some of the gas poor galaxies in the near distance slice could be former companions of M86 ejected at high speeds to relatively high clustercentric distances because of the falling of this subclump into the cluster (Paper II; Vollmer et al. 2001). The intermediate range of  $20 < d < 25$  Mpc is composed mainly of galaxies with moderate neutral gas deficiencies spreaded more or less uniformly over all the sky. Although the uncertainties in the distance estimates do not permit a neat separation of the different Virgo substructures, it is interesting to note that the majority of the objects in the HI-deficient galaxy clustering seen at 25–30 Mpc also have systemic velocities not dissimilar from those of the M87 subcluster (see Tables 2 and 3), in agreement with the original definition of the W' cloud given in VCC (note that the W cloud is underrepresented in TF datasets). On the other hand, the marginal indications of a galaxy enhancement in the NW of the 30–35-Mpc-distance slice might correspond to the M cloud, given that the candidate galaxies exhibit systemic velocities around  $2000 \text{ km s}^{-1}$ . Beyond 35 Mpc, galaxies become progressively scarce, although with an apparent tendency to reside in the peripheral W and M cloud regions. This picture is consistent with the claims that the W and M background clouds of Virgo are twice as far away as its central subunits, with the W' cloud being somewhat closer (e.g., Binggeli et al. 1987; YFO97; Gav99).

A final glance at Figure 5 also shows that the gas-deficient enhancement noted in Paper II around the region of the M cloud (see Fig. 1) is indeed the result of the chance superposition along the LOS of several spirals with substantial gas deficiency, but located at very different LOS distances and without any physical connection.

## 6.2. Cartesian Coordinates

A complementary characterization of the spatial structure of the Virgo region can be inferred from the projected distributions of the spiral galaxies into the three main planes of the cartesian three-dimensional space visualized in Figure 6. In the plots, the xy-plane is taken parallel to the equatorial plane (Decl. =  $0^\circ$ ), with the x- and y-axis pointing to R.A. = 12 and 18 hr, respectively, and the z-axis pointing to the north. In this coordinate system, the yz-plane is nearly perpendicular to the LOS to M87, i.e., it is roughly a tangent plane to the celestial sphere. The spherical coordinates have been transformed into linear coordinates at the distance of the individual galaxies listed in Table 3. As in previous figures, the symbol sizes are directly proportional to the HI deficiency of the galaxies and the large cross marks the position of M87.

This figure allows one to appreciate the true aspect of the spiral and HI distributions in the Virgo region. One remarkable feature of the galaxy distribution is that at large radial distances ( $\gtrsim 25$ –30 Mpc) it appears to split into two branches in the vertical direction of the xz-plane, which is roughly perpendicular to the plane of the Local Supercluster. The fact that the z-axis is nearly perpendicular to the LOS suggests that this galaxy arrangement is not an artifact produced by the uncertainty in the radial distances affecting for the most part the x direction. Notice also that the upper branch, which goes through M87 and embraces

the deficient objects having the most extremal radial distances, contains nearly all the galaxies with strong HI depletions, i.e., those with  $\text{DEF} > 2\sigma$ , or equivalently, with at least a factor three reduction in the HI mass. This upper filament of the spiral distribution is pretty well aligned with the chain of bright elliptical galaxies that defines the principal axis of Virgo (Arp 1968; West & Blakeslee 2000).

To complete our description of the three-dimensional distribution of the gaseous deficiency, we show in Figure 7 the surfaces of iso-HI deficiency corresponding to 1, 2, and 3 standard deviations from normalcy. These surfaces have been generated by a straightforward extension of the adaptive kernel method described in Silverman (1986) for smoothing galaxy number density distributions, also used in the determination of the HI-deficiency contours depicted in Figure 1. We observe in the panel corresponding to the  $1\sigma$ -level surface the presence of two disconnected condensations of HI deficiency: the elongated one in the front encompasses most of the HI-deficient galaxies associated with the main body of the cluster and the gas-poor objects nearest to us, while the most distant surface is related to the group of strongly gas-deficient galaxies that we have tentatively identified in the background of the Virgo cluster (compare this panel with Figs. 2 and 5). The remaining two panels illustrate the already commented fact that the highest gas deficiencies in the Virgo region are found in the front of the cluster. As explained in § 4, little bias seems to be caused by HI deficiency in the TF distances, even for extreme gas depletions, so the abundance of gas-poor objects at short radial distances from our position appears to be a real effect.

## 7. Summary and Remarks

In this paper, we have examined in more detail the suggestion presented in Paper II that, in addition to the main galaxy concentration around M87, some of the well-known peripheral Virgo groups also contain strongly gas-deficient spirals. The overall distribution of HI deficiency in the Virgo region has been compared with the three-dimensional galaxy distribution. The following conclusions have been reached:

(1) We confirm that the distribution of the spirals in the Virgo I cluster region is very elongated along the LOS; the galaxies associated with this region have LOS distances raging from less than 10 to more than 50 Mpc. The projected sky distribution of the Virgo spirals, however, looks (lumpy but) relatively compact, with a typical extent of only about 10 Mpc. The overall width-to-depth ratio is approximately 1 : 4, although with a strong east-west variability. The most distant objects concentrate in the western quadrant, while in the eastern half few spirals are seen at LOS distances larger than 25 Mpc. The Virgo filamentary structure appears to split into two branches around the  $W'$  cloud region.

(2) The distribution of spiral galaxies with significant HI deficiency is also characterized by great depth along the LOS. The highly gas-deficient spirals tend to concentrate along the upper branch of the spiral galaxy distribution, which is roughly aligned with the principal axis of the Virgo cluster.

(3) Within 4 Mpc of M87, the measured HI deficiency is essentially a monotonically decreasing function of the distance from that galaxy, in agreement with the behavior observed in other HI-deficient clusters. Moreover, in the Virgo region, significant HI deficiency enhancements are also identified at large distances from the Virgo core, well beyond the typical distance where the hot X-ray emitting ICM is concentrated. Tests of whether locally-high peripheral gas deficiencies are a rather common feature in cluster regions must await the equally-careful tracing of the HI deficiency, incorporating quality 3D distance measures around other clusters.

(4) While the principal peak in the distribution of HI deficiency arises from numerous gas-poor galaxies

coincident with the core and with LOS distances ranging from  $\sim 16$  to 22 Mpc, other important enhancements of the gas deficiency are associated with several nearby galaxies ( $d \lesssim 15$  Mpc) moving away from the cluster with large relative velocities, and with what appears to be a compact background group of galaxies between  $\sim 25$ –30 Mpc, most with roughly the same systemic velocities as the cluster mean, which matches the original definition of the  $W'$  cloud. In addition, we have demonstrated that the localized enhancement in DEF observed in the Virgo sky map around the M cloud position actually arises from several galaxies at very different distances aligned along the LOS and without any physical connection. In agreement with results presented by Dale et al. (2001), nothing in our analysis suggests that TF distance measurements are unreliable in objects with severe gas depletion.

Further progress in (1) and (2) needs a careful revision of TF distances —at least until Cepheid distance measurements in Virgo galaxies become more commonplace. Even after the elimination of systematic differences among published Virgo catalogs, a few galaxies still exhibit strongly inconsistent distance measurements: 16 of the 161 members of the 21-cm sample have  $1\sigma$  uncertainties larger than 5 Mpc. Nevertheless, although the details may be questioned, the general picture reporting the elongated structure of the distribution of both the spirals and their HI deficiency, as well as the clumped nature of the latter, should be correct. We can make a simple estimate of the *typical* elongation introduced by the uncertainty in the distances. The standard deviation of individual distances (0.29 mag) is likely responsible for an increase of  $\sim 40\%$  in the scale of the true LOS distance distribution by assuming an average distance of the spiral galaxies of 20 Mpc. Given that the absolute errors in distance increase with the values of this quantity, as it is obvious from inspection of Figure 2, one can expect an artificial increment of the depth by a somewhat larger factor for the most distant galaxies which, in any event, would be clearly insufficient to account for the very strong LOS elongation of the galaxy distribution.

On the other hand, results (3) and (4) have profound implications on our understanding of the gas removal events and the influence of the environment on the life of the galaxies. While the characteristics exhibited by the HI deficiency in cluster centers tend to support the interaction between the galaxies and the hot intracluster gas as the main cause of their gas depletion, our finding that a number of spirals with substantial HI deficiencies lie at large radial distances from the Virgo cluster center is hard to reconcile with the proposition that this environmental process is also the cause. At this stage, it would be desirable to investigate whether these peripheral deficient objects have been produced *in situ* by alternative gas deficiency mechanisms, such as galaxy-galaxy interactions, predicted to operate in galaxy groups. In this sense, it would be of importance to perform multi-wavelength observations of the HI-deficient subclump detected in the Virgo background. Model calculations show that tidal stresses in disks generate extended tail structures in the stellar and neutral hydrogen distributions, the latter with surface densities well above the detection threshold of the most sensitive aperture-synthesis radio observations. In contrast, gas depletion arising from the ram-pressure sweeping of the interstellar medium should produce a dearth of atomic gas in the outer portions of the disks, as well as bow shocks and dense gaseous tails observable in X-rays.

We are especially indebted to Pascal Fouqué for providing machine-readable versions of his TF data on the Virgo cluster and for his careful reading of an earlier version of the manuscript. Masataka Fukugita and Martin Federspiel have also generously contributed with their TF data to the making of our Virgo catalog. We are grateful to all the people and institutions that have made possible the LEDA (<http://leda.univ-lyon1.fr>). Sergi Gómez assisted with one of the figures. This work was supported by the Dirección General de Investigación Científica y Técnica, under contracts PB97–0411 and AYA2000–0951. J.M.S. would like also to thank the Departament d’Astronomia i Meteorologia at the Universitat de Barcelona where part

of this work was prepared. T.S. acknowledges support from a fellowship of the Ministerio de Educación, Cultura y Deporte of Spain. This work has been supported of US NSF grants AST96–17069 to R.G. and AST99–00695 to M.P.H. and R.G.

## REFERENCES

- Arp, H. 1968, *PASP*, 80, 129
- Binggeli, B., Popescu, C., & Tammann, G.A. 1993, *A&AS*, 98, 275
- Binggeli, B., Sandage, A., & Tammann, G.A. 1985, *AJ*, 90, 1681 (VCC)
- Binggeli, B., Tammann, G.A., & Sandage, A. 1987, *AJ*, 94, 251
- Böhringer, H., Briel, U.G., Schwarz, R.A., Voges, W., Hartner, G., & Trümper, J. 1994, *Nature*, 368, 828
- Bravo-Alfaro, H., Cayatte, V., van Gorkom, J.H., & Balkowski, C. 2000, *AJ*, 119, 580
- Cayatte, V., Kotanyi, C., Balkowski, C., & van Gorkom, J.H. 1994, *AJ*, 107, 1003
- Chamaraux, P., Balkowski, C., & Gérard, E. 1980, *A&A*, 83, 38
- Dale, D.A., Giovanelli, R., Haynes, M.P., Campusano, L.E., & Hardy, E. 1999, *AJ*, 118, 1489
- Dale, D.A., Giovanelli, R., Haynes, M.P., Hardy, E., & Campusano, L.E. 2001, *AJ*, 121, 1886
- de Lapparent, V., Geller, M.J. & Huchra, J.P. 1986, *ApJ*, 302, L1
- de Vaucouleurs, G. 1961, *ApJS*, 6, 213
- de Vaucouleurs, G., de Vaucouleurs, A., Corwin, H.G., Buta, R.J., Paturel, G., & Fouqué, P. 1991, *Third Reference Catalogue of Bright Galaxies* (New York: Springer) (RC3)
- Dressler, A. 1986, *ApJ*, 301, 35
- Ekholm T., Lanoix, P., Teerikorpi, P., Fouqué, P., & Paturel, G. 2000, *A&A*, 355, 835 (Ekh00)
- Federspiel, M., Tammann, G.A., & Sandage, A. 1998, *ApJ*, 495, 115 (FTS98)
- Fouqué, P., Bottinelli, L., Gouguenheim, L., & Paturel, G. 1990, *ApJ*, 349, 1 (Fou90)
- Fouqué, P., Solanes, J.M., Sanchis, T., & Balkowski, C. 2001, *A&A*, 375, 770
- Freedman, W.L., et al. 2001, *ApJ*, 553, 47
- Ftclas, C., Struble, M.F., & Fanelli, M.N. 1984, *ApJ*, 282, 19
- Fukugita, M., Okamura, S., & Yasuda, N. 1993, *ApJ*, 412, L13
- Gavazzi, G., Boselli, A., Scodreggio, M., Pierini, D., & Belsole, E. 1999, *MNRAS*, 304, 595 (Gav99)
- Giovanelli, R., & Haynes, M.P. 1985, *ApJ*, 292, 404
- Giovanelli, R., Haynes, M.P., Herter, T., Vogt, N.P., Da Costa, L.N., Freudling, W., Salzer, J.J., & Wegner, G. 1997, *AJ*, 113, 53

- Guhathakurta, P., van Gorkom, J.H., Kotanyi, C.G., & Balkowski, C. 1988, *AJ*, 96, 851
- Gunn, J.E., & Gott, J.R. 1972, *ApJ*, 176, 1
- Haynes, M.P., & Giovanelli, R. 1984, *AJ*, 89, 758
- Haynes, M.P., & Giovanelli, R. 1986, *ApJ*, 306, 466
- Huchtmeier, W.K., & Richter, O.G., 1989, *A General Catalog of HI Observations of Galaxies* (Berlin: Springer)
- Kraan-Korteweg, R.C., Cameron, L.M., & Tammann, G.A. 1988, *ApJ*, 331, 620 (KCT88)
- Magri, C., Haynes, M.P., Forman, W., Jones, C., & Giovanelli, R. 1988, *ApJ*, 333, 136
- Mould, J., Aaronson, M., & Huchra, J. 1980, *ApJ*, 238, 458 (MAH80)
- Neilsen, E.H., & Tsvetanov, Z.I. 2000, *ApJ*, 536, 255
- Pierce, M.J., & Tully, R.B. 1988, *ApJ*, 330, 579 (PT88)
- Quilis, V., Moore, B., & Bower, R. 2000, *Science*, 288, 1617
- Sakai, S., Mould, J.R., et al. 2000, *ApJ*, 529, 698
- Sanchis, T., Solanes, J.M., Salvador-Solé, E., Fouqué, P. 2002, *ApJ*, in press
- Schindler, S., Binggeli, B., & Böhringer, H. 1999, *A&A*, 343, 420
- Silverman, B. W. 1986, *Density Estimation for Statistics and Data Analysis* (London: Chapman and Hall)
- Solanes, J.M., Giovanelli, R., & Haynes, M.P. 1996, *ApJ*, 461, 609 (Paper I)
- Solanes, J.M., Manrique, A., González-Casado, G., García-Gómez, C., Giovanelli, R., & Haynes, M.P. 2001, *ApJ*, 548, 97 (Paper II)
- Teerikorpi, P., Bottinelli, L., Gouguenheim, L., & Paturel, G. 1992, *A&AS*, 260, 17
- Tully, R.B. 1982, *ApJ*, 257, 389
- Tully, R.B., & Fisher, J.R. 1977, *A&AS*, 54, 661 (TF)
- Vollmer, B., Cayatte, V., Balkowski, C., & Duschl, W.J. 2001, *ApJ*, 561, 708
- West, M.J., & Blakeslee, J.P. 2000, *ApJ*, 543, L27
- Yahil, A., Tammann, G.A., & Sandage, A. 1977, *ApJ*, 207, 903
- Yasuda, N., Fukugita, M., & Okamura, S. 1997, *ApJS*, 108, 417 (YFO97)

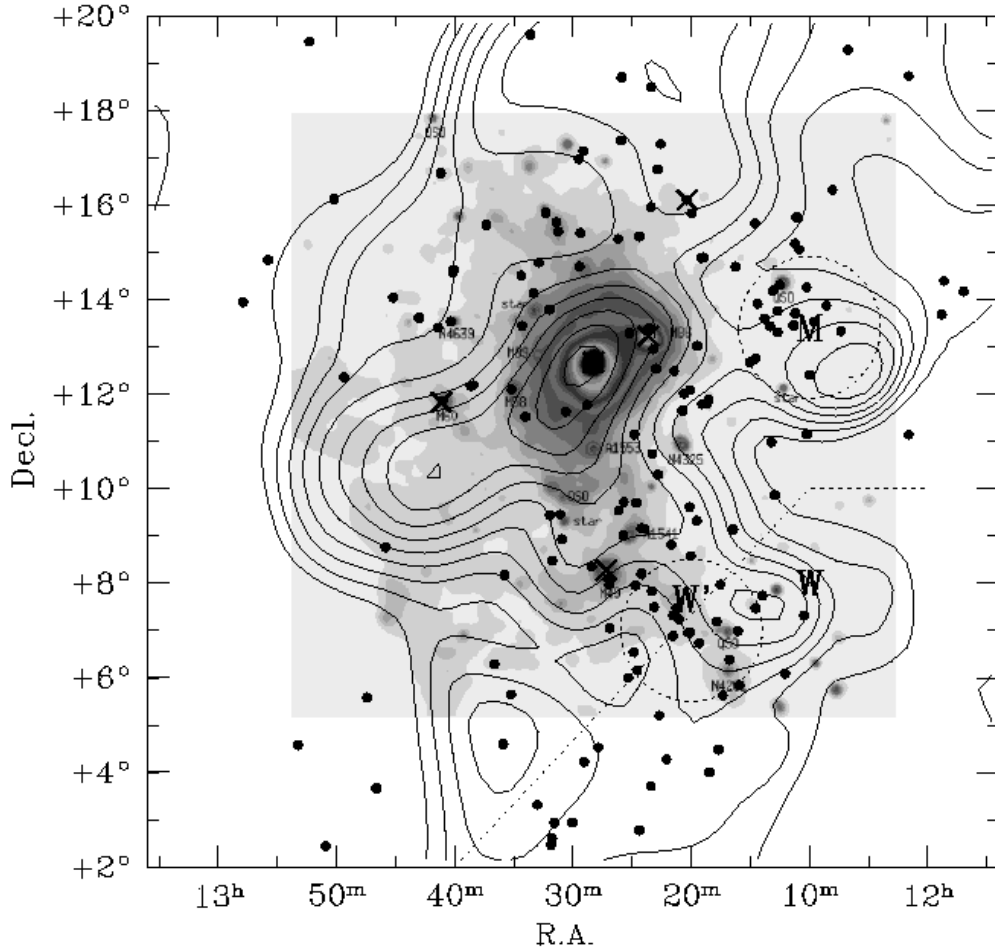


Fig. 1.— Distribution in celestial coordinates of the 161 members of the 21-cm sample (five galaxies with extreme values of declination have been omitted for a better overall impression). The contour map of the *distance-independent* HI deficiency parameter (see text) is reproduced from Paper II, and has been generated using a straightforward extension of the adaptive kernel technique described in Silverman (1986). Note that the contours are generated from all the 287 spirals with a neutral content measure listed in the AGC within the area depicted by the figure. A grey-scaled version of the X-ray image of the central cluster region in the ROSAT all-sky-survey in the hard (0.4–2.4 keV) energy band is overlaid also on the figure. The background W, W', and M subgroups from Binggeli et al. (1993) are delineated by dotted lines. The sky positions of five dominant galaxies are marked by crosses (top to bottom: M100, M86, M87, M60, and M49). The projected location of M87 coincides with the peak of the HI deficiency and of the X-ray emission.

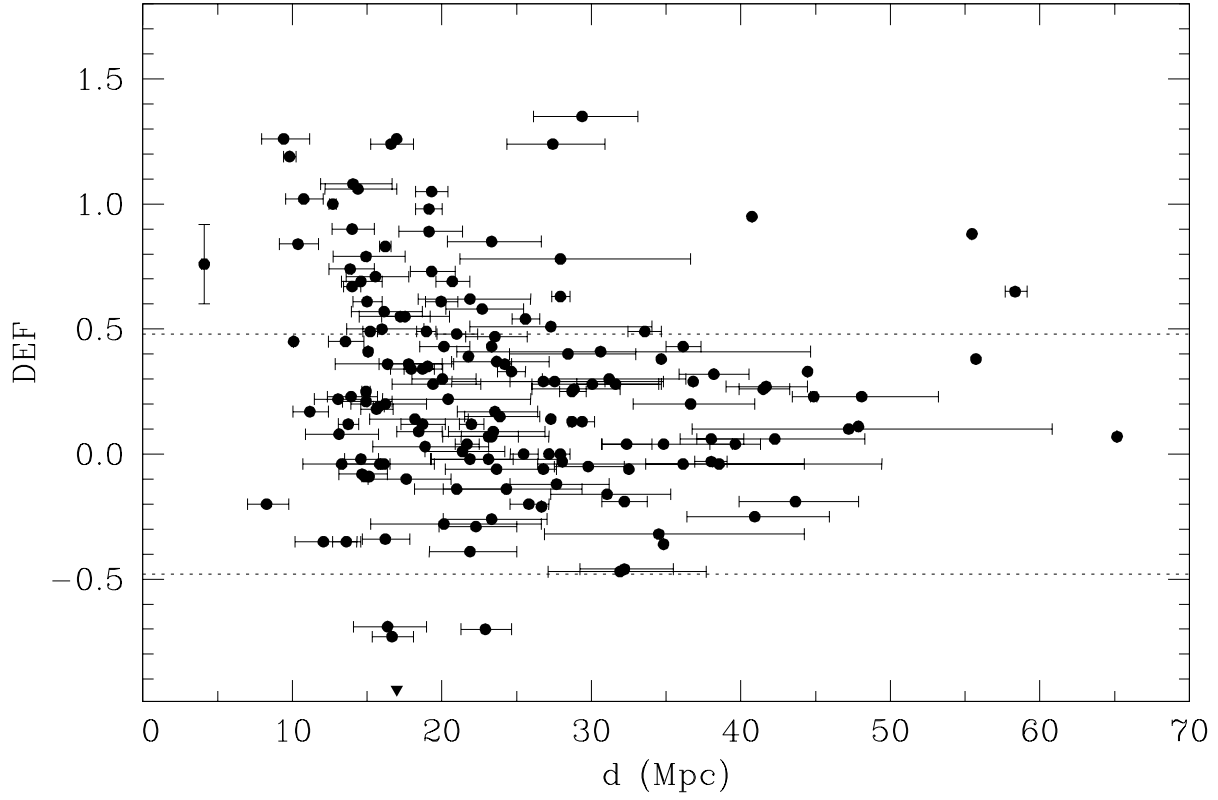


Fig. 2.— Individual values of DEF for the 161 members of the 21-cm sample as a function of the LOS distance. Dotted lines show 2 times the standard deviation shown by the values of this parameter in field galaxies. Horizontal error bars represent the  $1\sigma$  uncertainties of the distances quoted in the literature with respect to the calculated mean values. The filled triangle marks the distance to M87 quoted in LEDA. The vertical error bar in the point closest to us shows an estimate of the typical uncertainty of the individual values of DEF expected from random errors in the determination of the observables  $a_{\text{opt}}^2$ ,  $F_{\text{DEF}}^c$ , and  $T$ , that enter in the calculation of this parameter.



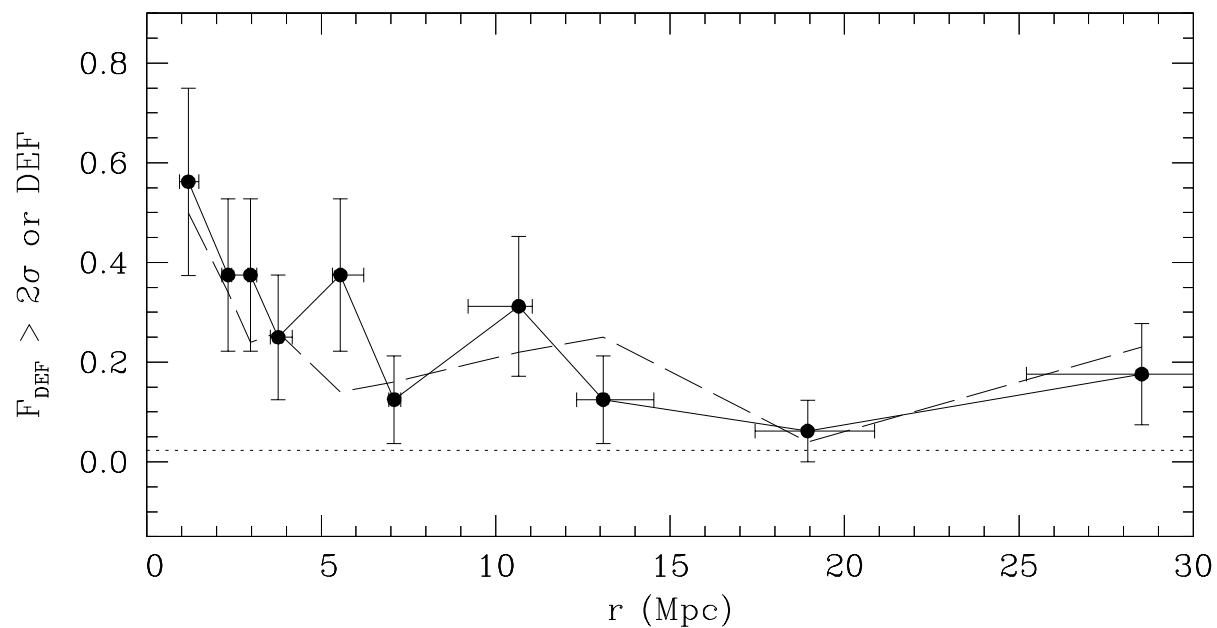


Fig. 3.— Data points illustrate the run of the fraction of spirals with  $\text{DEF} > 2\sigma$  with three-dimensional radial distance from the center of the Virgo cluster. Vertical error bars correspond to  $1\sigma$  confidence Poisson intervals. The abscissas show medians and interquartile ranges of the bins in distance determined from 16 galaxies, with the remainder one added to the last bin. The horizontal dotted line is the expectation value of  $F_{\text{DEF}}$  for field spirals if  $\text{DEF}$  follows a gaussian distribution. The long-dashed curve illustrates the radial run of the medians of the binned number distributions in the measured  $\text{DEF}$ .

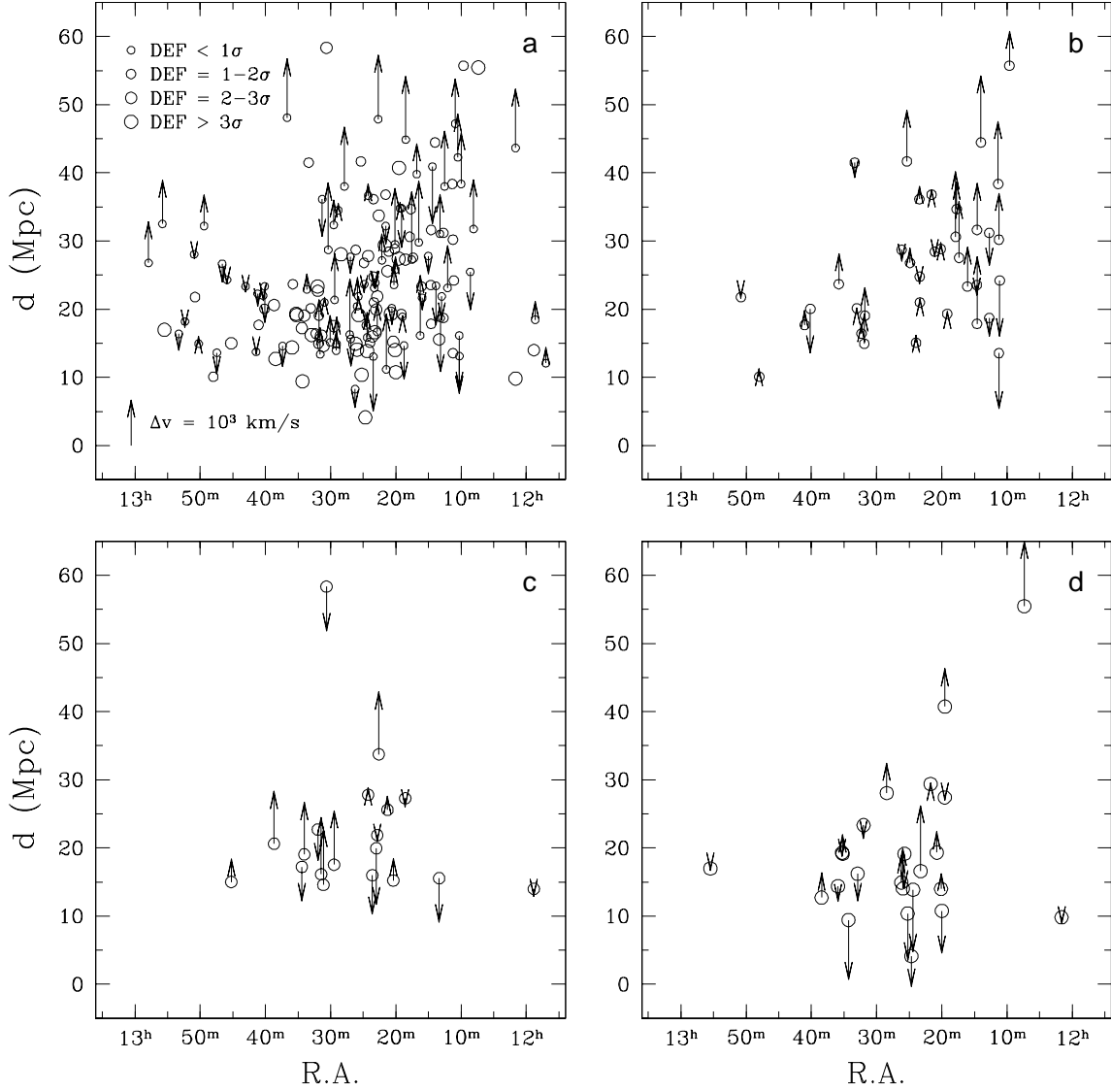


Fig. 4.— The distribution of the observed relative recessional velocities for different intervals of H I deficiency. The horizontal axis shows the position of the galaxy in Right Ascension while the vertical axis shows its LOS distance in Mpc. The size and orientation of the arrows indicates the radial velocity relative to the systemic cluster recessional velocity:  $\Delta v = v_{\text{sys}} - 980 \text{ km s}^{-1}$ . Panel (a) depicts all data points but only the velocities for non-H I-deficient galaxies ( $\text{DEF} < 1\sigma$ ). In the rest of panels, the H I-deficient galaxies are separated according to specific ranges of deficiency: (b)  $\text{DEF} = 1-2\sigma$ , (c)  $\text{DEF} = 2-3\sigma$ , and (d)  $\text{DEF} > 3\sigma$ . Two galaxies with  $d > 65$  Mpc have been excluded from the Figure.

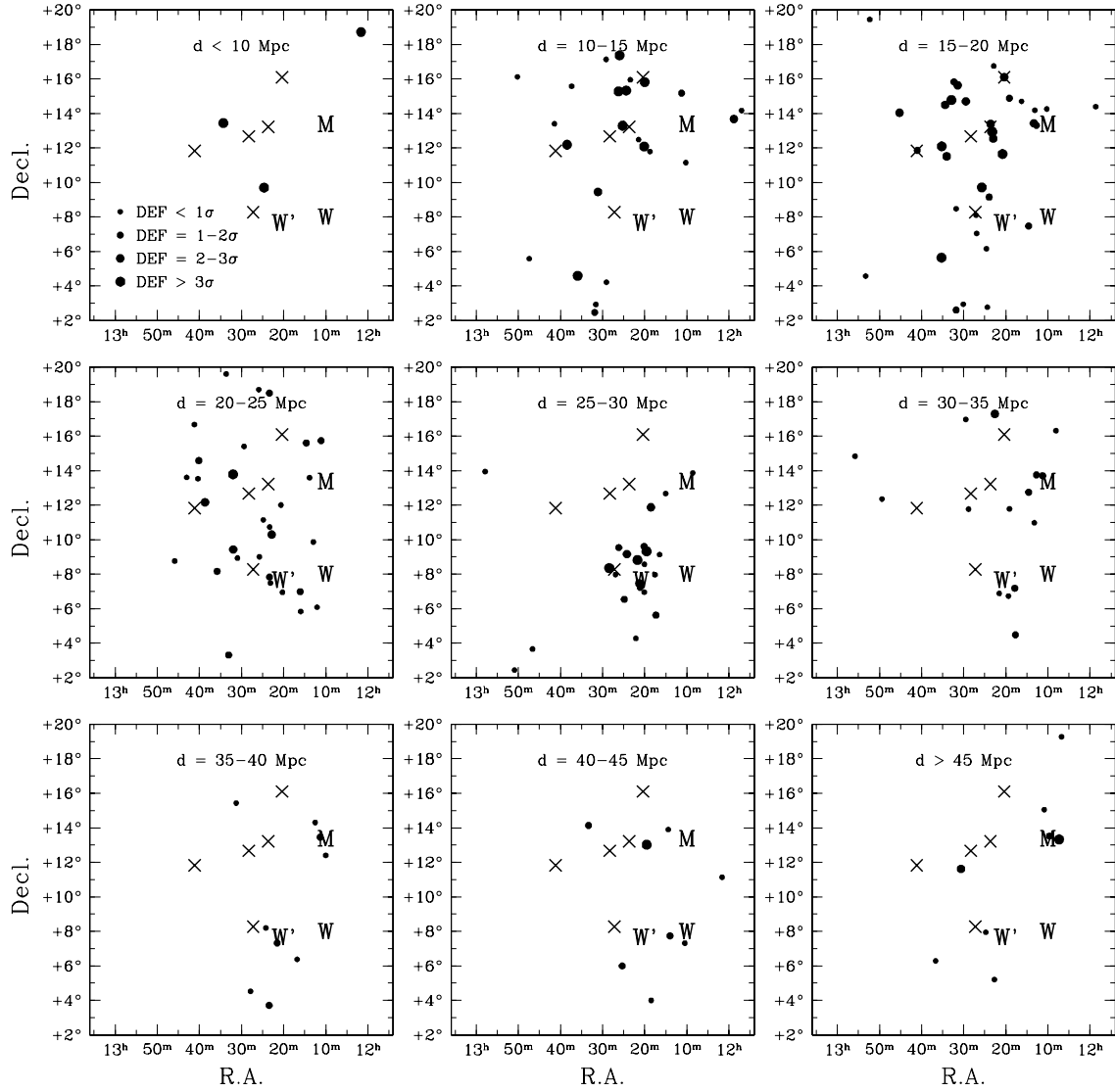


Fig. 5.— Sky distribution of the Virgo spirals for specific ranges of the LOS distance. All panels encompass a range of LOS distances of 5 Mpc, except for the first and last ones which encompass, respectively, all the objects with  $d < 10$  Mpc and with  $d > 45$  Mpc. The size of the symbols correlates with the HI deficiency of the galaxies (see the correspondences in the first panel) measured in units of the mean standard deviation for field objects ( $= 0.24$ ). Crosses and uppercase letters have the same meaning as in Fig. 1.

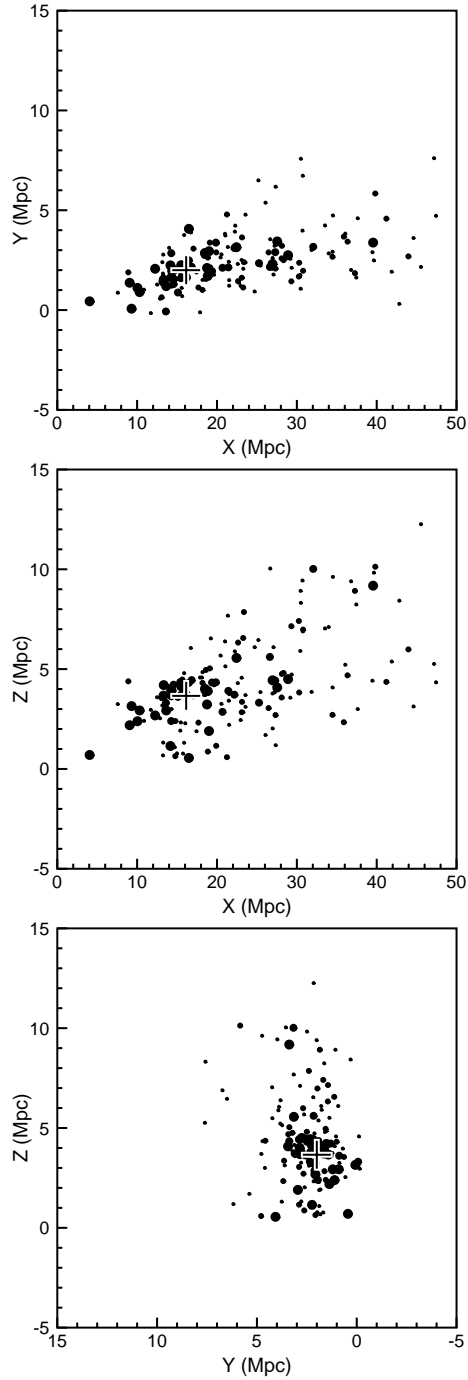


Fig. 6.— Distribution of the Virgo spirals in the three main planes of the rectangular equatorial coordinate system. The xy-plane corresponds to Decl. =  $0^\circ$ , the x- and y-axis point to R.A. = 12 and 18 hr, respectively, and the z-axis points to the north. As in Figure 5, the symbol size indicates the relative degree of HI deficiency. The large cross in each panel marks the position of M87.

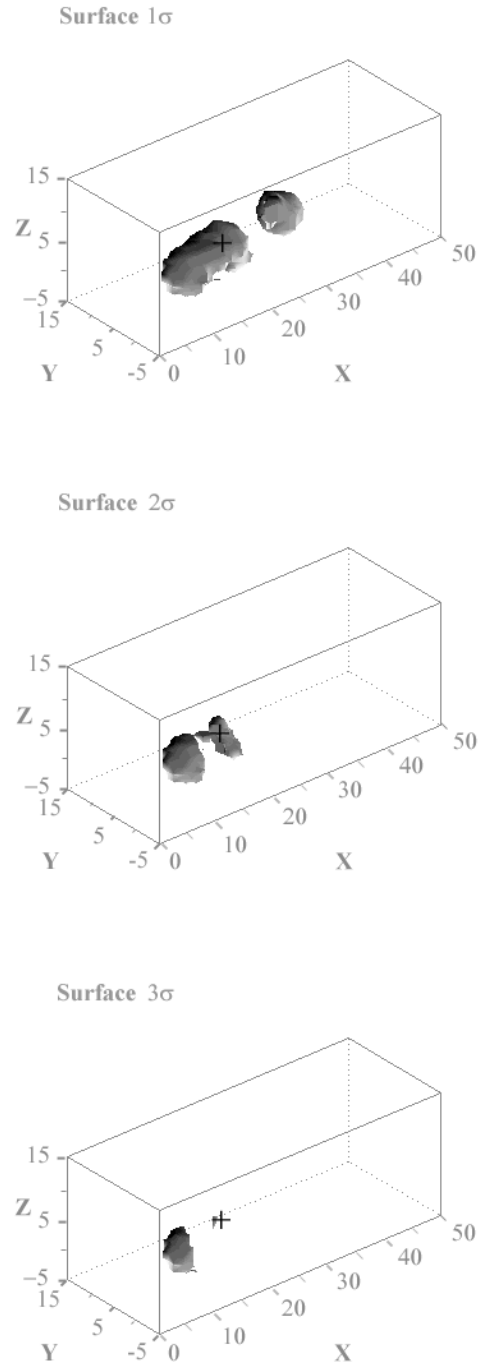


Fig. 7.— *Top to bottom:* Surfaces of iso-HI deficiency corresponding to 1, 2, and 3 standard deviations from normalcy. All plots are in rectangular equatorial coordinates as in Figure 6 with distances given in Mpc. The crosses mark the position of M87. Our position is at the origin of the coordinate system.

Table 1. TF Datasets Contributing to the Present Sample

Source	Acronym	Number of galaxies	
		Total	Selected
Yasuda, Fukugita, & Okamura 1997	YFO97	246	165
Mould, Aaronson, & Huchra 1980	MAH80	23	21
Pierce & Tully 1988	PT88	34	34
Kraan-Korteweg, Cameron, & Tammann 1988	KCT88	128	84
Fouqué et al. 1990	Fou90	178	145
Federspiel, Tammann, & Sandage 1998	FTS98	132	129
Gavazzi et al. 1999	Gav99	75	72
Ekhholm et al. 2000	Ekh00	96	52

Table 2. Distance Moduli for Individual Galaxies

VCC	NGC/ IC	UGC/ CGCG	R.A. (1950)	Decl. (1950)	T	Mem.	YFO97	MAH80	PT88	KCT88	Fou90	FTS98	Gav99	Ekh00	Ceph.	Distance modulus
(1)	(2)	(3)	(4)	(5)	(6)	(7)	(8)	(9)	(10)	(11)	(12)	(13)	(14)	(15)	(16)	(17)
...	...	CG69-10	11 57 00.8	+14 09 51	7	...	30.82	...	...	...	29.83	...	...	...	...	$30.41 \pm 0.37$
...	I0755	U7001	11 58 37.3	+14 23 13	3	...	31.63	...	...	...	31.03	31.20	...	...	...	$31.33 \pm 0.18$
...	N4037	U7002	11 58 50.6	+13 40 41	3	...	30.68	...	...	...	30.61	...	...	...	...	$30.73 \pm 0.09$
...	N4064	U7054	12 01 37.3	+18 43 16	1	...	29.94	...	...	30.18	...	29.97	...	...	...	$29.96 \pm 0.09$
...	N4067	U7048	12 01 38.2	+11 08 13	3	...	33.39	...	...	...	32.70	33.29	...	...	...	$33.20 \pm 0.20$
...	...	U7133	12 06 46.7	+19 16 31	7	...	...	...	...	...	...	33.99	...	...	...	34.07
V0015	I3021	U7149	12 07 21.6	+13 19 42	9	M	33.79	...	...	...	...	...	...	...	...	33.72
V0025	N4152	U7169	12 08 03.8	+16 18 45	5	...	32.27	...	...	...	32.00	...	32.85	33.05	...	$32.52 \pm 0.36$
V0034	I3033	U7181	12 08 37.2	+13 51 54	7	A	32.12	...	...	31.99	31.88	32.04	...	...	...	$32.03 \pm 0.08$
V0047	N4165	U7201	12 09 39.0	+13 31 30	2	M	33.80	...	...	...	...	...	...	...	...	33.73
V0058	I0769	U7209	12 09 59.4	+12 24 00	4	M	32.39	...	32.68	...	...	32.99	32.92	33.52	...	$32.93 \pm 0.30$
V0066	N4178	U7215	12 10 13.8	+11 08 48	7	...	30.51	31.02	30.52	29.44	30.22	30.78	30.86	30.59	...	$30.59 \pm 0.40$
V0067	I3044	U7216	12 10 15.6	+14 15 18	6	A	31.57	...	...	30.69	30.94	30.94	...	...	...	$31.05 \pm 0.34$
V0073	N4180	U7219	12 10 28.9	+07 19 01	2	W	33.33	...	...	...	32.50	33.53	32.72	33.57	...	$33.13 \pm 0.29$
V0081	...	U7223	12 10 53.0	+15 03 00	7	A	32.87	...	...	...	33.70	...	...	...	...	$33.37 \pm 0.55$
V0087	...	...	12 11 07.0	+15 43 54	9	A	31.92	...	...	32.02	31.75	...	...	...	...	$31.92 \pm 0.04$
V0089	N4189	U7235	12 11 14.4	+13 42 12	6	M	32.64	...	31.63	...	...	32.64	...	33.01	...	$32.39 \pm 0.31$
V0092	N4192	U7231	12 11 15.4	+15 10 23	3	A	30.81	30.67	30.65	30.55	30.59	30.98	30.36	31.17	...	$30.66 \pm 0.19$
V0097	N4193	U7234	12 11 21.0	+13 27 00	4	M	32.78	...	...	...	...	32.98	32.64	33.54	...	$32.91 \pm 0.13$
V0105	...	U7239	12 11 36.0	+08 03 00	10	...	32.08	...	...	...	32.61	...	...	...	...	$32.43 \pm 0.40$
V0119	...	U7249	12 12 05.4	+13 05 24	10	A	31.86	...	31.78	31.89	31.62	31.78	...	...	...	$31.85 \pm 0.10$
V0120	N4197	U7247	12 12 04.9	+06 05 01	6	...	31.82	...	...	31.89	31.68	31.56	31.91	...	...	$31.82 \pm 0.18$
V0126	I3059	U7254	12 12 22.8	+13 44 12	10	A	31.87	...	...	...	31.73	31.92	...	...	...	$31.89 \pm 0.05$
V0131	I3061	U7255	12 12 31.8	+14 18 24	5	M	33.11	...	...	...	32.75	32.70	...	33.37	...	$32.90 \pm 0.12$
V0132	...	...	12 12 32.3	+13 18 41	8	A	30.67	...	...	...	...	29.77	...	...	...	$30.16 \pm 0.47$
V0143	I3066	U7262	12 12 43.2	+13 45 06	4	A	32.89	...	...	...	32.33	32.04	...	...	...	$32.47 \pm 0.33$
V0145	N4206	U7260	12 12 44.4	+13 18 12	4	A	31.48	31.36	31.01	31.47	31.20	31.15	31.29	...	...	$31.36 \pm 0.15$

Table 2—Continued

VCC (1)	NGC/ IC (2)	UGC/ CGCG (3)	R.A. (1950) (4)	Decl. (1950) (5)	T (6)	Mem. (7)	YFO97 (8)	MAH80 (9)	PT88 (10)	KCT88 (11)	Fou90 (12)	FTS98 (13)	Gav99 (14)	Ekh00 (15)	Ceph. (16)	Distance modulus (17)
V0152	N4207	U7268	12 12 58.2	+09 51 48	6	...	31.87	...	...	32.00	31.65	31.75	31.08	...	...	31.70 ± 0.27
V0157	N4212	U7275	12 13 06.6	+14 10 48	5	A	31.36	...	31.45	31.54	31.23	31.23	31.04	31.98	...	31.36 ± 0.17
V0162	I3074	U7279	12 13 13.4	+10 58 36	8	...	32.51	...	32.64	32.49	32.01	32.21	...	...	...	32.46 ± 0.28
V0167	N4216	U7284	12 13 21.6	+13 25 36	3	A	31.13	30.81	30.81	30.73	31.23	31.35	30.65	31.34	...	30.96 ± 0.29
V0187	N4222	U7291	12 13 49.8	+13 35 12	6	A	31.80	...	...	31.87	31.70	31.46	...	32.91	...	31.85 ± 0.30
V0199	N4224	U7292	12 14 00.4	+07 44 20	1	W	33.30	...	...	...	...	...	...	...	...	33.24
V0213	I3094	U7305	12 14 23.4	+13 54 12	5	A	33.37	...	...	...	32.60	...	...	...	...	33.06 ± 0.25
V0222	N4235	U7310	12 14 35.7	+07 28 11	1	W	31.48	...	...	...	...	...	...	31.76	...	31.27 ± 0.18
V0224	I3099	U7313	12 14 37.2	+12 44 54	6	M	32.39	...	...	...	32.55	32.37	...	...	...	32.50 ± 0.19
V0226	N4237	U7315	12 14 38.2	+15 36 08	4	A	31.63	...	...	32.15	31.80	31.95	31.48	32.52	...	31.86 ± 0.19
V0241	I3105	U7326	12 15 01.2	+12 40 00	10	A	30.48	...	...	30.56	30.74	30.69	...	...	...	30.62 ± 0.20
V0267	I3115	U7333	12 15 26.4	+06 55 53	6	...	34.92	...	...	...	31.96	...	32.08	...	...	32.23 ± 0.05
V0289	N4252	U7343	12 15 57.6	+05 50 18	3	...	31.81	...	...	...	...	31.62	...	...	...	31.68 ± 0.08
V0297	...	CG42-1	12 16 05.4	+06 59 06	5	...	...	...	...	...	...	31.85	...	...	...	31.84
V0307	N4254	U7345	12 16 16.8	+14 41 42	5	A	30.56	...	31.28	...	30.54	31.42	...	...	...	31.04 ± 0.41
V0318	I0776	U7352	12 16 30.0	+09 08 06	8	...	32.36	...	32.24	32.27	31.99	32.58	...	...	...	32.37 ± 0.17
V0341	N4260	U7361	12 16 48.8	+06 22 40	1	W	33.14	...	...	...	...	...	...	33.42	...	32.99 ± 0.09
V0343	I3148	...	12 16 48.0	+08 09 00	8	W	31.93	...	...	...	...	...	...	...	...	31.88
V0382	N4273	U7380	12 17 22.3	+05 37 27	5	W	31.83	...	...	...	...	32.27	32.19	32.91	...	32.20 ± 0.25
V0393	N4276	U7385	12 17 34.7	+07 58 10	6	W	32.23	...	...	...	...	...	...	...	...	32.18
V0404	...	U7387	12 17 42.9	+04 28 47	7	W	...	...	...	...	...	32.67	...	...	...	32.70
V0415	...	CG42-36	12 17 52.8	+07 11 12	5	W	33.31	...	...	...	...	31.63	...	...	...	32.43 ± 0.82
V0449	N4289	U7403	12 18 30.0	+04 00 00	6	W	...	...	...	...	...	33.20	...	33.75	...	33.26 ± 0.01
V0453	...	...	12 18 33.0	+11 52 24	6	A	32.74	...	...	32.42	31.31	...	...	...	...	32.18 ± 0.48
V0460	N4293	U7405	12 18 41.1	+18 39 36	0	A	31.14	...	...	30.81	30.91	...	30.53	31.03	...	30.76 ± 0.32
V0465	N4294	U7407	12 18 45.0	+11 47 24	6	A	30.66	31.15	...	30.85	30.55	30.66	30.86	...	...	30.83 ± 0.24
V0483	N4298	U7412	12 19 00.6	+14 53 06	5	A	31.03	...	...	32.22	31.04	31.19	...	...	...	31.38 ± 0.44



Table 2—Continued

VCC (1)	NGC/ IC (2)	UGC/ CGCG (3)	R.A. (1950) (4)	Decl. (1950) (5)	T (6)	Mem. (7)	YFO97 (8)	MAH80 (9)	PT88 (10)	KCT88 (11)	Fou90 (12)	FTS98 (13)	Gav99 (14)	Ekh00 (15)	Ceph. (16)	Distance modulus (17)
V0491	N4299	U7414	12 19 07.8	+11 46 48	8	A	...	...	...	...	32.49	...	...	...	...	32.71
V0497	N4302	U7418	12 19 10.2	+14 52 36	5	A	...	...	...	31.82	31.53	31.51	30.78	32.01	...	31.44 ± 0.33
V0509	...	U7423	12 19 22.3	+06 43 43	9	W'	32.67	...	...	32.67	32.27	33.13	...	...	...	32.71 ± 0.27
V0512	...	U7421	12 19 23.0	+12 14 35	10	A	32.05	...	...	32.02	31.30	...	...	...	...	31.82 ± 0.21
V0514	...	U7424	12 19 25.2	+08 57 06	10	B	32.00	...	...	...	30.70	...	...	...	...	31.43 ± 0.52
V0522	N4305	U7432	12 19 31.2	+13 01 06	1	A	...	...	...	33.15	...	...	...	...	...	33.05
V0524	N4307	U7431	12 19 33.0	+09 19 06	3	B	...	...	...	32.75	31.91	32.02	32.05	32.49	...	32.19 ± 0.26
V0534	N4309	U7435	12 19 38.9	+07 25 20	-1	W'	32.26	...	...	...	31.61	...	...	...	...	32.02 ± 0.19
V0559	N4312	U7442	12 19 59.4	+15 48 58	2	A	30.46	...	...	...	30.03	...	29.84	...	...	30.16 ± 0.25
V0566	...	...	12 20 05.0	+08 34 24	9	W'	32.17	...	...	32.25	31.68	...	...	...	...	32.06 ± 0.11
V0567	I3225	U7441	12 20 06.5	+06 57 14	8	W	32.33	...	...	...	...	32.40	...	...	...	32.34 ± 0.06
V0570	N4313	U7445	12 20 06.6	+12 04 54	2	A	30.79	...	...	30.72	30.82	30.91	30.34	...	...	30.73 ± 0.22
V0576	N4316	U7447	12 20 10.2	+09 36 36	6	B	32.42	...	...	32.55	32.30	32.28	31.70	32.88	...	32.30 ± 0.22
V0593	I3229	U7448	12 20 18.0	+06 57 00	4	W'	32.07	...	...	...	31.83	31.52	...	...	...	31.86 ± 0.25
V0596	N4321	U7450	12 20 23.2	+16 06 00	4	A	30.45	...	31.32	...	30.41	30.91	30.82	30.94	30.91	30.91 ± 0.07
V0613	N4324	U7451	12 20 32.5	+05 31 36	-1	W	31.81	...	...	...	...	...	31.19	...	...	31.53 ± 0.23
V0620	I3239	...	12 20 37.8	+12 00 18	9	A	32.36	...	...	31.49	30.63	...	...	...	...	31.52 ± 0.61
V0630	N4330	U7456	12 20 45.0	+11 38 42	6	A	31.21	...	...	31.76	31.30	31.38	31.31	...	...	31.43 ± 0.17
V0656	N4343	U7465	12 21 05.0	+07 13 58	3	W'	32.75	...	...	...	32.24	32.39	31.71	32.54	...	32.27 ± 0.32
V0664	I3258	U7470	12 21 12.0	+12 45 18	10	A	30.18	...	...	...	30.50	31.57	...	...	...	30.80 ± 0.58
V0667	I3259	U7469	12 21 16.2	+07 27 49	8	W'	32.00	...	...	...	31.80	32.14	...	...	...	32.04 ± 0.08
V0688	N4353	...	12 21 24.0	+08 04 00	10	B	32.84	...	...	...	32.05	32.68	...	...	...	32.59 ± 0.23
V0692	N4351	U7476	12 21 29.4	+12 28 54	2	A	30.16	...	...	...	30.18	30.01	30.48	...	...	30.24 ± 0.23
V0697	I3267	U7474	12 21 33.0	+07 19 12	6	W'	32.89	...	...	...	...	...	...	...	...	32.83
V0699	I3268	U7477	12 21 34.7	+06 53 00	5	B	32.81	...	...	...	32.11	...	...	...	...	32.54 ± 0.21
V0713	N4356	U7482	12 21 42.1	+08 48 48	6	B	31.96	...	...	32.56	32.37	32.36	...	...	...	32.34 ± 0.26
V0737	...	CG42-86	12 22 06.6	+04 16 36	8	W	...	...	...	...	...	32.17	...	...	...	32.17

Table 2—Continued

VCC (1)	NGC/ IC (2)	UGC/ CGCG (3)	R.A. (1950) (4)	Decl. (1950) (5)	T (6)	Mem. (7)	YFO97 (8)	MAH80 (9)	PT88 (10)	KCT88 (11)	Fou90 (12)	FTS98 (13)	Gav99 (14)	Ekh00 (15)	Ceph. (16)	Distance modulus (17)
V0740	...	...	12 22 07.0	+08 46 47	10	B	33.22	...	...	32.75	32.21	...	...	...	...	32.75 ± 0.30
V0768	I3298	...	12 22 36.0	+17 17 00	4	...	32.79	...	...	...	32.34	32.59	...	...	...	32.63 ± 0.07
V0785	N4378	U7497	12 22 44.3	+05 12 13	1	W	33.46	...	...	...	...	...	...	...	...	33.40
V0787	N4376	U7498	12 22 45.3	+06 01 06	10	...	31.49	...	...	31.31	31.13	31.55	31.89	...	...	31.52 ± 0.29
V0792	N4380	U7503	12 22 49.8	+10 17 36	2	B	31.47	31.20	31.30	31.27	32.09	32.13	31.73	32.42	...	31.70 ± 0.37
V0801	N4383	U7507	12 22 53.8	+16 44 48	1	A	30.90	...	...	...	30.95	...	31.19	...	...	31.11 ± 0.18
V0809	I3311	U7510	12 23 00.6	+12 32 12	7	A	31.62	...	...	31.50	31.43	31.38	...	...	...	31.50 ± 0.12
V0827	I3322A	U7513	12 23 09.9	+07 29 36	6	B	31.94	31.51	31.74	32.18	32.12	31.66	31.58	32.29	...	31.89 ± 0.23
V0836	N4388	U7520	12 23 13.8	+12 56 18	3	A	31.11	31.09	30.75	30.84	30.89	31.13	31.13	32.05	...	31.10 ± 0.19
V0849	N4390	U7519	12 23 19.8	+10 43 48	5	A	31.45	...	...	...	31.21	32.15	32.09	...	...	31.82 ± 0.40
V0851	I3322	U7518	12 23 21.6	+07 50 00	6	B	31.72	...	...	31.67	31.57	31.43	...	...	...	31.61 ± 0.14
V0857	N4394	U7523	12 23 24.7	+18 29 30	3	A	31.93	...	...	...	31.83	...	...	...	...	31.96 ± 0.08
V0859	...	U7522	12 23 25.8	+03 42 30	6	W	...	...	...	...	...	32.69	...	33.37	...	32.79 ± 0.07
V0865	N4396	U7526	12 23 27.5	+15 56 55	7	A	30.58	...	...	30.62	30.25	30.33	31.00	...	...	30.58 ± 0.28
V0873	N4402	U7528	12 23 34.8	+13 23 24	3	A	31.13	...	...	31.31	30.81	31.06	30.29	32.07	...	31.02 ± 0.35
V0874	N4405	U7529	12 23 35.8	+16 27 26	0	...	31.52	...	...	...	30.15	30.63	...	...	...	30.80 ± 0.49
V0905	N4411A	U7537	12 23 56.4	+09 08 54	5	B	30.27	...	...	...	30.68	33.04	...	...	...	30.89 <sup>b</sup>
V0912	N4413	U7538	12 24 00.0	+12 53 18	2	A	30.95	...	...	30.45	31.01	31.29	31.01	...	...	30.97 ± 0.33
V0938	N4416	U7541	12 24 14.5	+08 11 51	6	B	33.12	...	...	...	32.36	...	...	...	...	32.82 ± 0.24
V0939	N4411B	U7546	12 24 15.0	+09 09 42	6	B	32.23	...	...	...	32.05	...	...	...	...	32.23 ± 0.05
V0950	I3356	U7547	12 24 21.6	+11 50 18	10	A	31.71	...	30.70	...	30.12	...	...	...	...	30.94 ± 0.55
V0952	...	...	12 24 22.7	+10 09 17	5	B	32.48	...	...	...	31.74	31.55	...	...	...	31.97 ± 0.37
V0957	N4420	U7549	12 24 24.6	+02 46 15	5	W	...	...	...	...	...	31.03	30.93	...	...	31.00 ± 0.01
V0958	N4419	U7551	12 24 25.1	+15 19 28	1	A	30.73	...	...	30.82	30.15	...	30.97	...	...	30.71 ± 0.24
V0971	N4423	U7556	12 24 36.2	+06 09 23	8	...	31.09	...	...	...	31.17	30.84	31.55	...	...	31.23 ± 0.34
V0975	...	U7557	12 24 36.0	+07 32 00	9	B	31.73	...	...	...	33.89	...	...	...	...	... <sup>a</sup>
V0979	N4424	U7561	12 24 40.2	+09 41 48	1	B	28.00	...	...	28.25	...	...	...	...	...	28.07 ± 0.09

Table 2—Continued

VCC	NGC/ IC	UGC/ CGCG	R.A. (1950)	Decl. (1950)	T	Mem.	YFO97	MAH80	PT88	KCT88	Fou90	FTS98	Gav99	Ekh00	Ceph.	Distance modulus
(1)	(2)	(3)	(4)	(5)	(6)	(7)	(8)	(9)	(10)	(11)	(12)	(13)	(14)	(15)	(16)	(17)
V0980	I3365	U7563	12 24 42.0	+16 12 00	10	A	31.05	...	...	31.25	30.76	30.71	...	...	...	30.95 ± 0.19
V0989	...	...	12 24 45.0	+07 56 54	7	W'	34.35	...	...	...	...	...	...	...	...	34.28
V0995	I3371	U7565	12 24 49.2	+11 08 36	6	A	32.16	...	...	31.99	31.95	31.33	...	...	...	31.87 ± 0.34
V1002	N4430	U7566	12 24 53.6	+06 32 23	3	B	32.76	...	...	...	31.35	...	...	...	...	32.14 ± 0.57
V1011	...	U7567	12 24 56.7	+07 55 17	10	B	32.53	...	...	32.31	31.70	...	...	...	...	32.21 ± 0.23
V1043	N4438	U7574	12 25 13.8	+13 17 06	1	A	...	29.79	...	...	29.79	30.51	30.26	30.80	...	30.08 ± 0.27
V1048	...	U7579	12 25 22.6	+05 59 50	8	W	33.03	...	...	...	33.07	33.01	...	...	...	33.10 ± 0.14
V1086	N4445	U7587	12 25 43.8	+09 42 48	2	B	31.54	...	...	...	31.29	31.30	31.26	...	...	31.41 ± 0.10
V1091	...	U7590	12 25 46.2	+09 00 18	4	B	31.79	...	...	32.03	31.67	31.25	...	...	...	31.70 ± 0.29
V1110	N4450	U7594	12 25 58.0	+17 21 40	2	A	30.77	30.22	30.67	30.43	30.56	31.35	30.51	31.88	...	30.74 ± 0.37
...	I3391	U7595	12 25 55.6	+18 41 32	6	...	31.07	...	...	...	31.86	...	...	...	...	31.55 ± 0.52
V1118	N4451	U7600	12 26 08.4	+09 32 06	3	B	32.23	...	31.97	...	32.04	32.37	32.16	...	...	32.29 ± 0.07
V1126	I3392	U7602	12 26 12.0	+15 16 40	2	A	31.00	...	...	...	31.13	30.82	30.36	...	...	30.87 ± 0.35
...	N4455	U7603	12 26 14.1	+23 06 01	7	...	29.85	...	...	29.96	...	29.20	...	...	...	29.59 ± 0.36
V1189	I3414	U7621	12 26 56.2	+07 02 50	8	B	31.24	...	...	31.01	30.58	31.01	...	...	...	30.97 ± 0.15
V1193	N4466	U7626	12 26 58.0	+07 58 20	2	B	32.31	...	...	31.90	32.33	32.21	...	...	...	32.21 ± 0.26
V1205	N4470	U7627	12 27 05.3	+08 05 56	1	...	30.82	...	...	...	30.77	31.13	31.26	...	...	31.05 ± 0.21
V1290	N4480	U7647	12 27 53.4	+04 31 27	5	W	...	...	...	...	...	32.94	32.64	33.36	...	32.90 ± 0.06
V1330	N4492	U7656	12 28 27.4	+08 21 13	1	B	31.69	...	...	...	32.61	...	...	...	...	32.23 ± 0.59
V1356	I3446	...	12 28 51.6	+11 46 00	9	A	33.48	...	...	32.62	31.91	...	...	...	...	32.69 ± 0.54
V1375	N4496A	U7668A	12 29 05.8	+04 12 56	8	W	...	...	...	...	...	...	...	...	30.86	30.86 ± 0.03
V1379	N4498	U7669	12 29 08.8	+17 07 46	6	A	30.82	30.34	30.36	30.63	30.72	30.98	30.99	...	...	30.72 ± 0.26
V1393	I0797	U7676	12 29 22.9	+15 24 00	6	...	31.49	...	...	...	31.60	31.37	31.83	...	...	31.65 ± 0.27
V1401	N4501	U7675	12 29 27.6	+14 41 42	3	A	31.20	31.12	31.25	31.13	30.82	31.58	30.87	31.98	...	31.22 ± 0.20
V1410	N4502	U7677	12 29 32.2	+16 57 47	6	A	32.53	...	...	32.80	32.25	...	...	...	...	32.55 ± 0.11
V1442	I3474	U7687	12 30 04.0	+02 56 18	7	W	...	...	...	...	...	30.95	...	...	...	30.90
V1450	I3476	U7695	12 30 10.8	+14 19 30	10	A	30.90	...	...	...	31.28	31.71	...	...	...	31.35 ± 0.36

Table 2—Continued

VCC	NGC/ IC	UGC/ CGCG	R.A. (1950)	Decl. (1950)	T	Mem.	YFO97	MAH80	PT88	KCT88	Fou90	FTS98	Gav99	Ekh00	Ceph.	Distance modulus
(1)	(2)	(3)	(4)	(5)	(6)	(7)	(8)	(9)	(10)	(11)	(12)	(13)	(14)	(15)	(16)	(17)
...	...	U7697	12 30 20.8	+20 27 40	6	...	...	...	...	...	...	32.28	...	...	...	32.29
V1486	I3483	...	12 30 39.0	+11 37 12	3	A	32.30	...	...	...	33.63	33.73	...	...	...	33.83 ± 0.03
V1508	N4519	U7709	12 30 57.6	+08 55 48	7	B	31.27	31.82	31.25	31.28	31.38	31.84	31.33	32.57	...	31.61 ± 0.32
V1516	N4522	U7711	12 31 07.8	+09 27 00	6	B	31.06	30.48	30.67	31.23	30.45	30.92	30.71	...	...	30.82 ± 0.20
V1524	N4523	U7713	12 31 18.0	+15 26 00	9	A	32.16	...	...	...	33.25	...	...	...	...	32.79 ± 0.68
V1532	I0800	U7716	12 31 25.8	+15 37 51	5	...	30.66	...	...	...	31.29	31.05	30.93	...	...	31.04 ± 0.32
V1540	N4527	U7721	12 31 35.5	+02 55 45	4	W	...	...	...	...	...	31.21	30.03	31.38	...	30.62 ± 0.47
V1554	N4532	U7726	12 31 46.7	+06 44 43	10	B	29.94	31.10	30.65	31.01	30.01	...	30.23	...	...	30.55 ± 0.46
V1555	N4535	U7727	12 31 47.9	+08 28 25	5	B	30.47	31.19	30.60	30.51	30.16	30.78	30.67	31.68	30.99	30.99 ± 0.05
V1557	N4533	U7725	12 31 48.7	+02 36 10	7	W	...	...	...	...	...	31.43	...	...	...	31.40
V1562	N4536	U7732	12 31 53.5	+02 27 50	4	W	...	...	...	...	...	30.74	30.65	...	30.87 <sub>∞</sub>	30.87 ± 0.04
V1566	I3517	U7733	12 31 58.8	+09 25 54	9	B	31.96	...	...	31.70	31.26	32.11	...	...	...	31.78 ± 0.25
V1569	I3520	...	12 32 00.0	+13 46 54	6	A	33.47	...	...	31.65	32.03	31.73	...	...	...	31.84 ± 0.29
V1575	I3521	U7736	12 32 06.8	+07 26 09	10	B	31.28	...	...	31.79	31.07	...	31.23	...	...	31.39 ± 0.18
V1581	...	U7739	12 32 13.0	+06 34 35	10	B	32.58	...	...	...	32.77	...	...	...	...	32.76 ± 0.23
V1588	N4540	U7742	12 32 20.1	+15 49 37	6	A	31.83	...	...	...	30.39	31.39	30.51	...	...	31.07 ± 0.52
V1605	...	...	12 32 42.5	+10 42 24	5	A	32.45	...	...	...	32.04	31.25	...	...	...	31.96 ± 0.53
V1615	N4548	U7753	12 32 55.2	+14 46 24	3	A	30.81	...	30.89	...	30.66	31.31	30.88	31.65	31.05	31.05 ± 0.05
V1624	N4544	U7756	12 33 03.3	+03 18 45	1	S	...	...	...	31.73	...	31.68	31.17	...	...	31.52 ± 0.18
V1644	...	...	12 33 21.0	+14 08 00	9	A	33.17	...	...	33.28	32.75	...	...	...	...	33.09 ± 0.09
...	N4561	U7768	12 33 38.4	+19 35 56	7	...	32.01	...	...	...	31.42	...	...	...	...	31.80 ± 0.16
V1673	N4567	U7777	12 34 01.2	+11 32 00	4	A	...	...	...	...	...	...	...	32.68	...	32.10
V1676	N4568	U7776	12 34 02.4	+11 30 54	4	A	...	...	...	...	...	31.36	...	32.10	...	31.39 ± 0.07
V1678	I3576	U7781	12 34 06.0	+06 54 00	9	B	33.30	...	...	...	30.41	...	...	...	...	... <sup>a</sup>
V1686	I3583	U7784	12 34 12.6	+13 32 00	10	A	30.17	...	...	31.17	30.46	...	30.68	...	...	30.66 ± 0.34
V1690	N4569	U7786	12 34 18.6	+13 26 24	2	A	29.77	29.56	...	29.49	29.69	30.05	30.37	31.03	...	29.87 ± 0.37
V1696	N4571	U7788	12 34 25.2	+14 29 48	6	A	30.99	...	30.55	...	30.84	31.70	31.41	...	...	31.18 ± 0.38

Table 2—Continued

VCC	NGC/ IC	UGC/ CGCG	R.A. (1950)	Decl. (1950)	T	Mem.	YFO97	MAH80	PT88	KCT88	Fou90	FTS98	Gav99	Ekh00	Ceph.	Distance modulus
(1)	(2)	(3)	(4)	(5)	(6)	(7)	(8)	(9)	(10)	(11)	(12)	(13)	(14)	(15)	(16)	(17)
V1699	I3591	U7790	12 34 29.9	+07 11 59	10	B	31.02	...	...	31.20	30.69	...	...	...	...	31.00 ± 0.09
V1725	...	...	12 35 09.0	+08 50 00	10	B	31.66	...	...	31.57	30.71	...	...	...	...	31.34 ± 0.30
V1726	...	U7795	12 35 13.0	+07 22 47	10	B	31.08	...	...	...	31.03	31.20	...	...	...	31.15 ± 0.09
V1727	N4579	U7796	12 35 12.0	+12 05 36	3	A	31.30	...	31.06	...	31.07	31.74	31.61	31.86	...	31.41 ± 0.24
V1730	N4580	U7794	12 35 15.6	+05 38 38	2	...	31.35	...	...	...	31.34	...	...	...	...	31.43 ± 0.12
V1758	...	U7802	12 35 48.0	+08 10 00	6	...	31.73	...	...	...	32.07	31.65	...	...	...	31.87 ± 0.30
V1760	N4586	U7804	12 35 55.1	+04 35 37	1	S	...	...	...	31.24	...	...	30.40	...	...	30.79 ± 0.36
V1780	N4591	U7821	12 36 39.9	+06 17 11	3	...	33.25	...	...	...	...	33.64	...	33.80	...	33.41 ± 0.22
V1791	I3617	U7822	12 36 53.0	+08 14 12	10	...	31.34	...	31.06	31.89	30.92	...	...	...	...	31.37 ± 0.26
V1811	N4595	U7826	12 37 20.9	+15 34 23	3	A	30.66	...	...	30.91	30.78	30.71	30.94	...	...	30.82 ± 0.17
V1859	N4606	U7839	12 38 26.4	+12 11 12	1	A	30.52	...	...	30.58	30.37	...	...	...	...	30.52 ± 0.04
V1868	N4607	U7843	12 38 40.8	+12 09 54	3	A	31.53	...	...	31.86	31.36	31.49	...	...	...	31.58 ± 0.12
V1923	N4630	U7871	12 39 58.5	+04 14 03	10	S	...	...	...	...	...	31.14	30.91	...	...	31.05 ± 0.06
V1929	N4633	U7874	12 40 06.6	+14 37 48	8	A	31.63	...	...	32.57	31.45	31.86	31.48	...	...	31.84 ± 0.33
V1932	N4634	U7875	12 40 10.2	+14 34 12	6	A	31.53	...	...	...	31.59	31.27	...	...	...	31.51 ± 0.23
V1933	...	...	12 40 12.5	+07 36 42	2	...	32.82	...	...	...	32.49	...	...	...	...	32.73 ± 0.02
V1943	N4639	U7884	12 40 21.0	+13 31 54	4	A	31.74	...	31.57	32.07	31.74	32.55	32.00	32.53	31.71	31.71 ± 0.08
V1955	N4641	U7889	12 40 36.0	+12 19 24	-2	A	29.64	...	...	...	29.17	...	...	...	...	29.50 ± 0.12
V1972	N4647	U7896	12 41 01.2	+11 51 12	5	A	...	...	30.65	...	31.09	31.57	31.19	31.95	...	31.25 ± 0.26
...	N4651	U7901	12 41 12.5	+16 40 05	5	...	31.57	31.45	31.58	31.46	31.46	32.16	...	32.57	...	31.74 ± 0.25
V1987	N4654	U7902	12 41 26.4	+13 24 00	6	A	30.56	30.79	30.43	30.74	30.51	30.74	30.75	31.41	...	30.69 ± 0.11
V2023	I3742	U7932	12 43 01.2	+13 36 24	5	A	31.69	...	...	31.90	31.37	31.73	32.25	...	...	31.84 ± 0.32
V2058	N4689	U7965	12 45 15.0	+14 02 06	5	A	30.75	...	30.64	...	30.64	31.06	...	31.74	...	30.88 ± 0.14
V2070	N4698	U7970	12 45 51.8	+08 45 37	1	...	32.80	31.28	31.77	31.73	32.03	...	31.53	32.35	...	31.93 ± 0.41
...	N4701	U7975	12 46 39.0	+03 39 45	6	...	...	...	...	...	...	...	...	32.71	...	32.13
...	N4713	U7985	12 47 25.6	+05 34 58	7	...	30.92	...	...	30.63	...	30.65	...	...	...	30.67 ± 0.15
...	N4725	U7989	12 47 59.9	+25 46 20	2	...	...	...	...	...	...	...	...	30.78	30.46	30.46 ± 0.06

Table 2—Continued

VCC (1)	NGC/ IC (2)	UGC/ CGCG (3)	R.A. (1950) (4)	Decl. (1950) (5)	T (6)	Mem. (7)	YFO97 (8)	MAH80 (9)	PT88 (10)	KCT88 (11)	Fou90 (12)	FTS98 (13)	Gav99 (14)	Ekh00 (15)	Ceph. (16)	Distance modulus (17)
...	N4746	U8007	12 49 25.2	+12 21 18	3	...	32.43	...	...	...	32.34	32.59	...	33.15	...	$32.54 \pm 0.10$
...	N4758	U8014	12 50 14.8	+16 07 10	9	...	30.57	30.62	...	31.19	30.95	30.93	...	...	...	$30.87 \pm 0.24$
...	N4771	U8020	12 50 48.5	+01 32 30	6	...	...	...	...	...	...	...	...	32.31	...	31.69
...	N4772	U8021	12 50 55.9	+02 26 27	1	...	...	...	...	...	...	...	...	32.81	...	32.24
...	I3881	U8036	12 52 20.2	+19 26 55	6	...	31.90	...	...	31.08	...	31.11	...	...	...	$31.30 \pm 0.39$
...	N4808	U8054	12 53 17.0	+04 34 28	6	...	...	...	...	31.49	...	30.80	...	...	...	$31.07 \pm 0.32$
...	N4845	U8078	12 55 28.1	+01 50 42	2	...	...	...	...	...	...	...	...	31.81	...	31.15
...	...	U8085	12 55 47.8	+14 49 52	6	...	...	...	...	...	...	32.54	...	...	...	32.56
...	...	U8114	12 57 54.4	+13 56 35	3	...	...	...	...	...	...	32.14	...	...	...	32.14

Note. — Col. (1)–(3): Galaxy names according to VCC, NGC or IC, and UGC or CGCG.

Col. (4) & (5): Galaxy coordinates. Units of right ascension are hours, minutes, and seconds. Units of declination are degrees, arcminutes, and arcseconds.

Col. (6): Morphological type index defined in RC3.

Col. (7): Membership given in VCC and Binggeli et al. (1993). M: member; A/B: clusters A/B; W/W'/M: clouds W/W'/M; S: southern extension.

Col. (8)–(15): Distance modulus to each galaxy given in each of the data sets listed in Table 1.

Col. (16): Distance modulus from Cepheids given by Freedman et al. (2001).

Col. (17): Mean distance modulus and  $1\sigma$  uncertainty resulting from the homogenization of the data sets (see text).

<sup>a</sup> All individual measures of the distance modulus rejected in the homogenization procedure.

<sup>b</sup> All but one individual measure of the distance modulus rejected in the homogenization procedure.

Table 3. Parameters for the Members of the 21-cm Sample

Galaxy Name (1)	$v_{\text{sys}}$ ( $\text{km s}^{-1}$ ) (2)	d (Mpc) (3)	$\langle DEF \rangle$ (4)	DEF (5)	$W_{20}^c$ ( $\text{km s}^{-1}$ ) (6)	Flag (7)	$M_{BT}^c$ (8)
Z69-10	1330	$12.08^{+2.24}_{-1.89}$	-0.19	-0.35	107	w	-15.83
I0755	1388	$18.45^{+1.59}_{-1.47}$	0.21	0.09	231	H	-17.69
N4037	814	$14.00^{+0.59}_{-0.57}$	0.88	0.67	190	i	-17.96
N4064	837	$9.82^{+0.42}_{-0.40}$	1.39	1.19	226	...	-18.15
N4067	2281	$43.65^{+4.21}_{-3.77}$	-0.08	-0.19	422	...	-20.56
U7133	2486	65.16	-0.05	0.07	260	o,W	-19.26
V0015	2406	55.46	0.77	0.88	227	o	-19.45
V0025	2062	$31.92^{+5.76}_{-4.80}$	-0.45	-0.47	379	i,s	-19.91
V0034	145	$25.47^{+0.96}_{-0.89}$	0.04	0.00	159	...	-17.46
V0047	1742	55.72	0.40	0.38	342	o	-19.74
V0058	2110	$38.55^{+5.71}_{-4.91}$	-0.19	-0.04	323	s	-20.00
V0066	242	$13.12^{+2.65}_{-2.24}$	0.02	0.08	296	...	-19.54
V0067	-299	$16.22^{+2.75}_{-2.31}$	0.23	0.20	171	...	-17.41
V0073	1933	$42.27^{+6.04}_{-5.21}$	0.05	0.06	460	s	-20.43
V0081	1963	$47.21^{+13.61}_{-10.46}$	0.01	0.10	209	i,s	-17.80
V0087	-242	$24.21^{+0.45}_{-0.48}$	0.36	0.36	151	...	-16.86
V0089	2004	$30.06^{+4.61}_{-4.04}$	0.20	0.28	438	...	-20.32
V0092	-246	$13.55^{+1.24}_{-1.14}$	0.26	0.45	479	...	-20.61
V0097	2356	$38.19^{+2.36}_{-2.31}$	0.20	0.32	388	...	-20.35
V0120	1910	$23.12^{+2.00}_{-1.82}$	-0.01	0.07	295	...	-19.52
V0131	2201	$38.02^{+2.16}_{-2.09}$	0.05	0.06	315	...	-19.86
V0143	264	$31.19^{+5.12}_{-4.45}$	0.54	0.30	177	H,s	-17.74
V0145	584	$18.71^{+1.34}_{-1.22}$	0.16	0.34	295	...	-19.76
V0152	456	$21.88^{+2.90}_{-2.60}$	0.00	-0.02	267	...	-18.71
V0157	-200	$18.71^{+1.52}_{-1.44}$	0.17	0.12	368	...	-19.98
V0162	1847	$31.05^{+4.27}_{-3.78}$	-0.22	-0.16	238	...	-18.17
V0167	16	$15.56^{+2.22}_{-1.94}$	0.53	0.71	533	...	-21.02
V0187	114	$23.44^{+3.47}_{-3.00}$	0.02	0.09	248	...	-19.46
V0199	2448	44.46	0.25	0.33	575	o	-20.74
V0213	-278	$40.93^{+5.00}_{-4.54}$	-0.12	-0.25	308	i,s	-18.98
V0222	2453	$17.95^{+1.55}_{-1.39}$	0.35	0.34	343	H	-19.23
V0224	2011	$31.62^{+2.89}_{-2.60}$	0.22	0.28	227	...	-18.89
V0226	756	$23.55^{+2.15}_{-1.95}$	0.54	0.47	330	...	-19.81
V0267	584	$27.93^{+0.65}_{-0.64}$	-0.01	0.00	644	...	-18.50
V0289	709	$21.68^{+0.81}_{-0.79}$	0.37	0.04	180	...	-17.37
V0297	1847	23.33	0.54	0.43	170	o,W	-17.04

Table 3—Continued

Galaxy Name (1)	$v_{\text{sys}}$ ( $\text{km s}^{-1}$ ) (2)	d (Mpc) (3)	$\langle DEF \rangle$ (4)	DEF (5)	$W_{20}^c$ ( $\text{km s}^{-1}$ ) (6)	Flag (7)	$M_{B_T}^c$ (8)
V0307	2303	$16.14^{+3.35}_{-2.76}$	−0.04	−0.04	452	i	−20.90
V0318	2328	$29.79^{+2.43}_{-2.25}$	−0.09	−0.05	236	...	−18.28
V0341	1649	$39.63^{+1.68}_{-1.70}$	−0.03	0.04	536	H	−20.63
V0382	2219	$27.54^{+3.36}_{-2.99}$	0.32	0.29	365	...	−20.29
V0393	2473	27.29	0.13	0.14	273	i,o	−18.54
V0404	1574	34.67	0.32	0.38	268	o,W	−19.24
V0415	2413	$30.62^{+14.05}_{-9.63}$	0.49	0.41	200	s	−17.08
V0449	2377	$44.87^{+0.21}_{-0.20}$	0.06	0.23	371	W	−20.47
V0453	785	$27.29^{+6.75}_{-5.41}$	0.56	0.51	127	s,w	−16.14
V0465	239	$14.66^{+1.71}_{-1.54}$	−0.08	−0.08	244	...	−19.04
V0483	1016	$18.88^{+4.24}_{-3.48}$	0.08	0.03	318	...	−19.92
V0491	112	34.83	−0.40	−0.36	349	i,o,W	−19.91
V0497	1034	$19.41^{+3.19}_{-2.72}$	0.27	0.28	383	...	−20.39
V0509	1109	$34.83^{+4.61}_{-4.11}$	0.03	0.04	181	...	−17.53
V0522	1814	40.74	0.92	0.95	457	H,o,W	−20.13
V0524	913	$27.42^{+3.49}_{-3.07}$	1.16	1.24	490	W	−20.33
V0559	47	$10.76^{+1.31}_{-1.19}$	1.19	1.02	232	...	−18.39
V0566	1267	$25.82^{+1.34}_{-1.27}$	−0.14	−0.20	117	w	−16.79
V0567	2215	$29.38^{+0.82}_{-0.86}$	0.11	0.13	233	...	−18.12
V0570	1319	$14.00^{+1.49}_{-1.33}$	1.04	0.90	280	...	−18.94
V0576	1117	$28.84^{+3.08}_{-2.80}$	0.19	0.26	334	...	−19.84
V0593	1392	$23.55^{+2.87}_{-2.52}$	0.47	0.17	159	H	−17.31
V0596	1468	$15.21^{+0.50^a}_{-0.49}$	0.32	0.49	482	i	−21.12
V0620	622	$20.14^{+6.53}_{-4.90}$	−0.13	−0.28	130	s,w	−16.40
V0630	1438	$19.32^{+1.57}_{-1.44}$	0.65	0.73	279	...	−19.35
V0656	868	$28.44^{+4.52}_{-3.92}$	0.40	0.40	401	...	−19.92
V0667	1279	$25.59^{+0.96}_{-0.89}$	0.53	0.54	212	...	−18.39
V0692	2203	$11.17^{+1.25}_{-1.13}$	0.60	0.17	164	i	−17.47
V0697	1085	36.81	0.30	0.29	280	i,o	−18.68
V0699	579	$32.21^{+3.27}_{-2.97}$	−0.31	−0.46	295	i	−18.44
V0713	998	$29.38^{+3.74}_{-3.25}$	1.28	1.35	302	...	−19.42
V0737	1566	27.16	0.02	0.00	164	o,W	−17.95
V0768	2354	$33.57^{+1.10}_{-1.12}$	0.61	0.49	212	H	−18.71
V0785	2395	47.86	−0.17	0.11	624	i,o	−21.00
V0792	840	$21.88^{+4.06}_{-3.47}$	0.60	0.62	346	...	−19.51
V0801	1608	$16.67^{+1.44}_{-1.32}$	−0.42	−0.73	302	...	−18.84



Table 3—Continued

Galaxy Name (1)	$v_{\text{sys}}$ ( $\text{km s}^{-1}$ ) (2)	d (Mpc) (3)	$\langle DEF \rangle$ (4)	DEF (5)	$W_{20}^c$ ( $\text{km s}^{-1}$ ) (6)	Flag (7)	$M_{BT}^c$ (8)
V0809	−262	$19.95^{+1.13}_{-1.05}$	0.62	0.61	178	...	−17.89
V0827	847	$23.88^{+2.67}_{-2.36}$	0.07	0.15	306	...	−19.53
V0836	2420	$16.60^{+1.52}_{-1.36}$	1.14	1.24	401	...	−20.17
V0849	972	$23.12^{+4.68}_{-3.86}$	0.06	−0.02	236	i	−18.73
V0851	1061	$20.99^{+1.40}_{-1.31}$	0.46	0.48	216	...	−18.59
V0857	823	$24.66^{+0.93}_{-0.95}$	0.27	0.33	432	i	−20.41
V0859	1265	$36.14^{+1.18}_{-1.15}$	0.33	0.43	321	W	−19.94
V0865	−228	$13.06^{+1.80}_{-1.57}$	0.22	0.22	202	...	−18.54
V0873	121	$16.00^{+2.80}_{-2.35}$	0.57	0.50	298	...	−19.27
V0905	1146	15.07	0.52	0.41	147	i,w	−17.43
V0938	1244	$36.64^{+4.28}_{-3.83}$	0.15	0.20	417	i	−19.80
V0939	1135	$27.93^{+0.65}_{-0.57}$	0.53	0.63	328	i	−19.16
V0957	1530	$15.85^{+0.07}_{-0.07}$	0.07	−0.04	232	W	−18.76
V0958	−380	$13.87^{+1.62}_{-1.43}$	0.92	0.74	307	...	−19.19
V0971	942	$17.62^{+2.99}_{-2.55}$	−0.08	−0.10	191	...	−18.45
V0979	314	$4.11^{+0.17}_{-0.18}$	1.32	0.76	108	w	−15.99
V0989	1704	71.78	0.12	0.13	195	i,o	−18.52
V0995	797	$23.66^{+4.01}_{-3.43}$	−0.06	−0.06	172	...	−17.57
V1002	1301	$26.79^{+8.04}_{-6.12}$	0.27	0.29	420	i,s	−19.48
V1043	−45	$10.38^{+1.37}_{-1.23}$	0.73	0.84	398	W	−19.56
V1048	2102	$41.69^{+2.78}_{-2.67}$	0.23	0.27	251	...	−19.14
V1086	230	$19.14^{+0.90}_{-0.88}$	1.11	0.98	240	...	−18.61
V1091	983	$21.88^{+3.13}_{-2.71}$	−0.16	−0.39	203	...	−18.06
V1110	1861	$14.06^{+2.61}_{-2.18}$	1.06	1.08	405	...	−20.14
I3391	1618	$20.42^{+5.52}_{-4.39}$	0.29	0.22	183	i,s	−18.03
V1118	725	$28.71^{+0.94}_{-0.85}$	0.43	0.25	308	...	−19.35
V1126	1571	$14.93^{+2.61}_{-2.20}$	1.08	0.79	228	...	−18.44
N4455	576	$8.28^{+1.49}_{-1.27}$	−0.12	−0.20	160	...	−16.77
V1189	381	$15.63^{+1.12}_{-1.04}$	0.24	0.18	170	...	−17.31
V1193	616	$27.67^{+3.52}_{-3.12}$	0.15	−0.12	237	...	−18.24
V1205	2200	$16.22^{+1.65}_{-1.54}$	0.07	−0.34	206	...	−18.34
V1290	2281	$38.02^{+1.07}_{-1.10}$	−0.04	−0.03	366	W	−20.28
V1330	1638	$27.93^{+8.72}_{-6.71}$	0.85	0.78	297	i,s	−19.19
V1356	1129	$34.51^{+9.74}_{-7.65}$	−0.27	−0.32	228	s	−17.94
V1375	1581	$14.86^{+0.21a}_{-0.20}$	−0.11	−0.09	303	W	−19.09
V1379	1411	$13.93^{+1.77}_{-1.57}$	0.22	0.23	234	...	−18.58

Table 3—Continued

Galaxy Name (1)	$v_{\text{sys}}$ ( $\text{km s}^{-1}$ ) (2)	d (Mpc) (3)	$\langle DEF \rangle$ (4)	DEF (5)	$W_{20}^c$ ( $\text{km s}^{-1}$ ) (6)	Flag (7)	$M_{B_T}^c$ (8)
V1393	1995	$21.38^{+2.83}_{-2.52}$	0.06	0.01	219	...	-18.37
V1401	2167	$17.54^{+1.69}_{-1.56}$	0.40	0.55	603	...	-21.55
V1410	1531	$32.36^{+1.68}_{-1.65}$	0.04	0.04	225	...	-18.58
V1442	1572	15.14	-0.06	-0.09	154	H,o,W	-17.71
U7697	2454	28.71	0.09	0.13	215	o,W	-17.10
V1486	6	$58.34^{+0.81}_{-0.67}$	0.65	0.65	180	H	-18.82
V1508	1093	$20.99^{+3.33}_{-2.83}$	-0.21	-0.14	287	i	-19.37
V1516	2199	$14.59^{+1.41}_{-1.30}$	0.65	0.69	257	...	-18.82
V1524	158	$36.14^{+13.29}_{-9.72}$	-0.13	-0.04	299	i,s	-18.98
V1532	2237	$16.14^{+2.56}_{-2.20}$	0.72	0.57	151	i	-17.29
V1540	1571	$13.30^{+3.22}_{-2.60}$	-0.14	-0.04	410	W	-19.99
V1555	1825	$15.78^{+0.37a}_{-0.36}$	0.16	0.19	397	i	-20.64
V1557	1596	19.05	0.34	0.35	187	o,W	-18.18
V1562	1641	$14.93^{+0.28a}_{-0.27}$	0.08	0.25	394	W	-20.43
V1566	295	$22.70^{+2.77}_{-2.44}$	0.61	0.58	133	w	-17.04
V1569	687	$23.33^{+3.33}_{-2.95}$	0.90	0.85	215	...	-16.50
V1588	1184	$16.37^{+4.43}_{-3.51}$	0.39	0.36	338	i	-18.82
V1615	383	$16.22^{+0.38a}_{-0.37}$	0.77	0.83	410	i	-20.38
V1624	992	$20.14^{+1.74}_{-1.63}$	0.57	0.43	212	W	-18.01
V1644	646	$41.50^{+1.76}_{-1.62}$	0.23	0.26	114	w	-16.26
N4561	1324	$22.91^{+1.75}_{-1.63}$	-0.67	-0.70	293	...	-19.23
V1676	2125	$18.97^{+0.62}_{-0.64}$	0.35	0.49	248	W	-20.43
V1690	-328	$9.42^{+1.75}_{-1.47}$	1.13	1.26	401	...	-20.28
V1696	235	$17.22^{+3.29}_{-2.75}$	0.48	0.55	311	i	-19.58
V1727	1397	$19.14^{+2.24}_{-2.02}$	0.75	0.89	594	i	-21.18
V1730	893	$19.32^{+1.10}_{-1.08}$	1.17	1.05	283	i	-18.84
V1758	1651	$23.66^{+3.51}_{-3.01}$	0.37	0.37	185	...	-18.03
V1760	639	$14.39^{+2.59}_{-2.20}$	1.15	1.06	292	W	-18.72
V1780	2279	$48.08^{+5.13}_{-4.63}$	0.17	0.23	399	s	-19.88
V1811	530	$14.59^{+1.19}_{-1.10}$	0.34	-0.02	204	...	-18.37
V1859	1528	$12.71^{+0.24}_{-0.24}$	1.25	1.00	224	...	-18.27
V1868	2138	$20.70^{+1.18}_{-1.09}$	0.73	0.69	245	...	-18.89
V1929	185	$23.33^{+3.83}_{-3.27}$	0.06	0.07	228	...	-18.83
V1932	11	$20.04^{+2.24}_{-2.05}$	0.28	0.30	291	...	-19.51
V1943	873	$21.98^{+0.82a}_{-0.80}$	0.09	0.12	375	...	-19.90
V1972	1297	$17.78^{+2.26}_{-1.97}$	0.42	0.36	345	i,W	-19.58

Table 3—Continued

Galaxy Name (1)	$v_{\text{sys}}$ (km s <sup>-1</sup> ) (2)	d (Mpc) (3)	$\langle DEF \rangle$ (4)	DEF (5)	$W_{20}^c$ (km s <sup>-1</sup> ) (6)	Flag (7)	$M_{B_T}^c$ (8)
N4651	705	22.28 <sup>+2.72</sup> <sub>-2.45</sub>	-0.29	-0.29	472	...	-20.81
V1987	926	13.74 <sup>+0.71</sup> <sub>-0.67</sub>	0.06	0.12	365	...	-20.13
V2023	856	23.33 <sup>+3.71</sup> <sub>-3.24</sub>	-0.17	-0.26	205	...	-18.44
V2058	1493	15.00 <sup>+1.00</sup> <sub>-0.95</sub>	0.65	0.61	320	i	-19.55
V2070	882	24.32 <sup>+5.05</sup> <sub>-4.23</sub>	-0.20	-0.14	663	s	-20.79
N4701	574	26.67	-0.30	-0.21	272	i,o,W	-19.55
N4713	511	13.61 <sup>+0.97</sup> <sub>-0.90</sub>	-0.35	-0.35	280	i	-18.66
N4725	1163	12.36 <sup>+0.35</sup> <sub>-0.34</sub>	0.21	0.45	510	W	-20.68
N4746	1669	32.21 <sup>+1.52</sup> <sub>-1.49</sub>	-0.18	-0.19	365	...	-20.08
N4758	1150	14.93 <sup>+1.74</sup> <sub>-1.56</sub>	0.21	0.21	207	...	-18.60
N4771	959	21.78	0.31	0.39	293	o,W	-19.88
N4772	883	28.05	-0.07	-0.03	510	o,W	-20.56
I3881	849	18.20 <sup>+3.58</sup> <sub>-3.01</sub>	0.08	0.14	249	...	-18.77
N4808	616	16.37 <sup>+2.60</sup> <sub>-2.28</sub>	-0.68	-0.69	265	W	-19.60
N4845	940	16.98	1.20	1.26	596	o,W	-19.90
U8085	1943	32.51	-0.14	-0.06	246	o,W	-19.16
U8114	1887	26.79	0.11	-0.06	157	o,W	-16.90

Note. — Col. (2): Radial velocities from HI measurements referred to the kinematic frame of the Local Group.

Col. (3): Distance and  $1\sigma$ -errors.

<sup>a</sup> Distance from Cepheids. Errors are those quoted by Freedman et al. (2001).

Col. (4) & (5): HI deficiency parameters defined in the text.

Col. (6): Edge-on HI line width.

Col. (7): H: non-AGC flux or non-detection corrected only for internal HI self-absorption; i:  $i < 45^\circ$  (from LEDA); o: distance based on a single non-Cepheid measurement; s:  $1\sigma$  uncertainties in the distance larger than 5 Mpc; W: corrected HI line width *not* from YFO97; w:  $100 < W_{20}^c < 150$  km s<sup>-1</sup> (see text for further details).

Col. (8): Total absolute corrected  $B$ -magnitude calculated from the absorption-free brightness given in LEDA.